A Precision Measurement of the Neutral Pion Lifetime via the Primakoff Effect

Proposal Update for E-99-014

May 28, 2002

A. Ahmidouch, S. Danagoulian (spokesperson),
A. Gasparian (spokesperson and contact person), C. Jackson, S. Mtingwa, J. Underwood
North Carolina A&T State University, Greensboro, NC

E. Clinton, R. Hicks, D. Lawrence, R. Miskimen (spokesperson)
University of Massachusetts, Amherst, MA

D. Dale (spokesperson), M. Gabrielyan, B. Hu, W. Korsch, A. Teymurazyan, P. Zolnierczuk
University of Kentucky, Lexington, KY

A. Afanasev, E. Chudakoff, H. Egiyan, R. Ent, V. Gyurjyan, M. Ito, J.P. Chen,
Y. Sharabian, E. Smith
Thomas Jefferson National Accelerator Facility, Newport News, VA

K. Baker, M. Christy, J. Goity, P. Gueye, C. Keppel, L. Tang, L. Yuan
Hampton University, Hampton, VA

L. Gan, M. Alexanian, T. Black
University of North Carolina at Wilmington, Wilmington, NC

A.M. Bernstein, D. Hasell, S. Kowalski, R. Suleiman
Massachusetts Institute of Technology, Cambridge, MA

D. Sober, H. Crannell, R. Hakobyan
The Catholic University of America, Washington, DC

J. Ball, M. Dugger, E. Pasyuk, B.G. Ritchie
Arizona State University, Tempe, AZ

R. Minehart, B. Stevens
University of Virginia, Charlottesville, VA

A. Asratyan, O. Chernyshov, G. Davidenko, A. Dolgolenko, G. Dzyubenko, A. Evdokimov,
V. Goryachev, A. Kamenskii, M. Kubantsev, I. Larin, V. Matveev, V. Semyachkin,
A. Sitnikov, V. Verebryusov, V. Vishnyakov
Institute for Theoretical and Experimental Physics, Moscow, Russia

Yu. Goncharenko, V. Kubarovsky, A. Meschanin, L. Soloviev, A. Vasiliev
Institute for High Energy Physics, Protvino, Russia

M. Khandaker, V. Punjabi, C. Salgado
Norfolk State University, Norfolk, VA

A. Glamazdin, A. Omelaenko
Kharkov Institute of Physics and Technology, Kharkov, Ukraine

P.L. Cole
University of Texas at El Paso, El Paso, TX

A. Nathan
University of Illinois, Urbana, IL

C. Li, Z. Liu, S. Lu, J. Yuan, J. Zhou, S. Zhou, X. Zhu
Chinese Institute of Atomic Energy, Beijing, China

J. He
Institute of High Energy Physics, Chinese Academy of Sciences, Beijing, China

W. Briscoe
George Washington University, Washington, DC

I. Aznauryan, S. Gevorgyan, A. Margaryan, K. Egiyan,
H. Voskanyan, A. Ketikyan, A. Shahinyan, A. Petrosyan
Yerevan Physics Institute, Yerevan, Armenia

B. Milbrath
Eastern Kentucky University, Richmond, KY

A.I. Fix, V.A. Tryasuchev
Tomsk Polytechnical University, Tomsk, Russia

M. Elaasar
Southern University at New Orleans, New Orleans, LA

Contents

1 Theoretical Developments **5**

2 Previous experiments **7**
2.1 The direct method . . . 7
2.2 Measurements using $\gamma\gamma$ collisions . . . 9
2.3 Measurements using the Primakoff effect . . . 9

3 Overview of the Experiment **10**

4 Accomplishments and Technical Readiness **11**
4.1 Funding and Contributions of Major Capital Equipment . . . 11
4.2 Beamline Instrumentation . . . 14
4.2.1 The Total Absorption Counter for Flux Monitoring . . . 14
4.2.2 Harp . . . 15
4.3 PrimEx Targets . . . 15
4.4 The PrimEx/Hall B Pair Spectrometer . . . 17
4.4.1 Dipole and Vacuum Box . . . 18
4.4.2 Results from Magnet Mapping . . . 18
4.4.3 Detectors . . . 19
4.5 The Hybrid Calorimeter - HYCAL . . . 20
4.5.1 Lead Glass Detectors . . . 22
4.5.2 Beam Test Results for the Lead Tungstate Detectors . . . 24
4.5.3 Energy Resolution . . . 26
4.5.4 Position Resolution . . . 27
4.5.5 Gain Change *versus* Radiation Dose Rate . . . 28
4.5.6 The Calorimeter Frame and Transporter . . . 30
4.5.7 The HYCAL Light Monitoring System . . . 31
4.5.8 Veto Scintillators . . . 37
4.6 Electronics and Data Acquisition . . . 38
4.6.1 High Voltage . . . 39
4.6.2 Trigger and HV Slow-Controls . . . 41
4.6.3 Custom Delay and Trigger Cables . . . 42
4.6.4 Trigger Design . . . 43
4.6.5 Expected Background and Trigger Rates . . . 43
4.7 Energy Calibration . . . 46

5 Summary **52**

Abstract

The PrimEx (Primakoff Experiment) Collaboration is preparing to perform a high precision (1.4%) measurement of the two photon decay width of the neutral pion, $\Gamma_{\pi^o \to \gamma\gamma}$. This measurement will provide a stringent test of the predictions of the U(1) axial anomaly in quantum chromodynamics. Photons from the Hall B photon tagging facility will be used to produce neutral pions in the Coulomb field of a nucleus. The two photons from the pion decay will be detected in a hybrid calorimeter (HYCAL) which will utilize lead tungstate ($PbWO_4$) scintillating crystals as well as lead glass Cherenkov shower counters. In addition to the development of this state-of-the-art calorimeter detector, a major experimental challenge in this measurement involves control of the luminosity. As such, extensive studies of the photoproduction targets have been performed, and a pair production luminosity monitor, which is now a part of the standard beamline in Hall B, has been constructed and is currently being commissioned. The physics goals of this experiment remain unchanged. However, recent theoretical developments in ChPT, inspired by the original proposal, provide greater impetus for performing such a high precision measurement. Here, we discuss the progress which has been made since E-99-014 was approved by PAC 15, and thereby request from PAC 22 that this experiment remain approved.

1 Theoretical Developments

The two-photon decay mode of the π^0 reveals one of the most profound symmetry issues in quantum chromodynamics, namely, the explicit breaking of a classical symmetry by the quantum fluctuations of the quark fields coupling to a gauge field[1]. This phenomenon, called anomalous symmetry breaking, is of pure quantum mechanical origin. In QCD, there are several observable phenomena that originate from anomalies. One is connected with the couplings of the quarks to the gluons. This is the so called axial anomaly by which the conservation of the axial U(1) symmetry of the classical Lagrangian of QCD is broken even in the limit where two or more quarks are massless, and the so called anomalous divergence of the corresponding axial-vector current becomes proportional to the product $\vec{E}^a \cdot \vec{B}^a$ of the chromo-electric and chromo-magnetic fields. The axial anomaly of interest to us involves the corresponding coupling of the quarks to photons[2]. In the limit of exact isospin symmetry, the π^o couples only to the isotriplet axial-vector current $\bar{q} I_3 \gamma_\mu \gamma_5 q$, where $q = (u,\ d)$, and I_3 is the third isospin generator. If we limit ourselves to two quark flavors, the electromagnetic current is given by $\bar{q}(1/6 + I_3/2)\gamma_\mu q$. When coupling to the photon, the isosinglet and isotriplet components of the electromagnetic current lead to an anomaly that explicitly breaks the symmetry associated with the axial-vector current $\bar{q}\ I_3\ \gamma_\mu \gamma_5\ q$, and this in turn directly affects the coupling of the π^o to two photons. The conservation of the axial U(1) current, to which the η' meson couples, as well as the $\bar{q}\frac{1}{2}\lambda_8 \gamma_\mu \gamma_5 q$, to which the η meson couples, are similarly affected by the electromagnetic field.

In the limit of vanishing quark masses, the anomaly leads to the $\pi^0 \to \gamma\gamma$ decay amplitude [1, 2]:

$$\mathcal{A}(\pi^0 \to \gamma\gamma) = \frac{\alpha_{em}}{4\pi F_\pi} \epsilon_{\mu\nu\rho\sigma} k^\mu k'^\nu \epsilon^{*\rho} \epsilon^{*\sigma}, \tag{1}$$

or the reduced amplitude,

$$A_{\gamma\gamma} = \frac{\alpha_{em}}{\pi F_\pi} = 2.513 \cdot 10^{-2} GeV^{-1} \tag{2}$$

where $F_\pi = 92.42 \pm 0.25 MeV$ [3] is the pion decay constant, and k and ϵ are respectively photon momenta and polarization vectors.

The width of the $\pi^o \to \gamma\gamma$ decay predicted by this amplitude is

$$\Gamma = M_\pi^3 \frac{\mid A_{\gamma\gamma} \mid^2}{64\pi} = 7.725 \pm 0.044 eV, \tag{3}$$

with a 0.6% uncertainty due to the experimental error in F_π. The current experimental value is 7.84 ± 0.56 eV[3] and is in good agreement with the predicted value with the chiral limit amplitude. This number is an average of several experiments[3] which will be discussed in Section 2. The error of 7% quoted by the Particle Data Book is most likely too low since each of the quoted experiments appears to have understated their errors and also, as can be seen in figure 1, from the much larger dispersion between the different measurements. Even at the 7% level the accuracy is not sufficient for a test of such a fundamental quantity, and in particular for the new calculations which take the finite quark masses into account. The level of precision of $\simeq 1.4\%$, which is the goal of PrimEx, will satisfy these requirements.

The decay amplitude given above is exact only in the chiral limit, *i.e.*, when the $u-$ and $d-$quark masses vanish. In this case, the anomaly is saturated by the π^o pole and the result for the decay amplitude given above is exact. However, the current-quark masses are non-vanishing and are approximately $m_u \simeq 4MeV$ and $m_d \simeq 7MeV$[6]. There are two sources of corrections due to this explicit breaking of chiral symmetry. The first and dominant one results from a combined effect that involves the corrections to the decay constants (because of isospin breaking there is a decay constant matrix in the subspace of the π^0, η and η') and an isospin breaking mixing that gives the physical π^0 a non-vanishing component along the pure U(3) states η and η'. In the absence of isospin breaking this source of chiral symmetry breaking boils down to merely replacing the value of F_π in the chiral limit by the measured value determined from π^+ decay[4, 5]. The second source of corrections is due to the fact that the saturation of the matrix elements of the divergence of the axial current also involves excited mesonic states when chiral symmetry is broken by quark masses. This effect is estimated using QCD sum rules[10] and turns out to be much smaller than the mixing effects.

Stimulated by the PrimEx proposal, calculations of the chiral corrections have been performed in the combined framework of chiral perturbation theory (ChPT) and the $1/N_c$ expansion up to $\mathcal{O}(p^6)$ and $\mathcal{O}(p^4 \times 1/N_c)$ in the decay amplitude[7][8]. The η' is explicitly included in the analysis as it plays as important a role as the η in the mixing effects. It was found that the decay width is enhanced by about 4% with respect to the value stated in equation (1). This enhancement is almost entirely due to the mixing effects. The result of this next-to-leading order analysis is $\Gamma_{\pi^0\to\gamma\gamma} = 8.10$ eV with an estimated uncertainty of less than 1%. Another theoretical calculation of the chiral corrections, also inspired by the PrimEx experiment, is also almost complete[9].

The quantity $1/R = (m_d - m_u)/m_s$ which enters into these calculations is of considerable interest, since it characterizes the size of the SU(2) breaking in the quark mass matrix. However, it is notoriously difficult to extract reliably. The standard procedure is to utilize the kaon mass difference, and to subtract the electromagnetic component of the mass difference using Dashen's theorem (kaon and pion EM mass shifts are identical in the chiral limit). When this procedure is followed one obtains $R \simeq 42$. Explicit calculations of the kaon-pion EM mass difference by Donoghue, Holstein, and Wyler and by Bijnens show a significant breaking of Dashen's theorem, and they conclude that $m_d - m_u$ is larger than what is given by the usual analysis, with $R \simeq 30$. There is also evidence from the $\eta \to 3\pi$ reaction that $m_d - m_u$ is underestimated by the conventional Dashen's theorem analysis. In summary, at the present time the precise size of the parameter R is difficult to determine. An important feature of the $\pi^0 \to \gamma\gamma$ decay rate is that it depends upon R in a known way, and that a precise measurement of the lifetime, as proposed in the PrimEx experiment, could provide a useful and independent value for this interesting and important parameter.

The proposed measurement at the $\simeq$1.4% accuracy level fills an important experimental gap, namely a precision verification of the predictions of the axial anomaly and the chiral corrections to the decay rate. As we shall show in the next section on previous experiments, the direct determination of $\Gamma_{\pi^0\to\gamma\gamma}$ lies below the prediction of the axial anomaly[13] and is therefore even more in disagreement with the new predictions which include the chiral corrections[7]. This makes the PrimEx experiment even more compelling and is arguably one of the most fundamental experiments that can be performed with few GeV electrons. It is

indeed extremely important that effects of chiral symmetry breaking by the $u-$ and $d-$quark masses, which can be rather precisely predicted theoretically, can actually be experimentally tested thanks to the projected level of precision of PrimEx. This would indeed be one of the most precise tests of fundamental aspects of QCD, namely anomalies and chiral symmetry breaking by quark masses, ever achieved.

2 Previous experiments

In view of the fundamental nature of the axial anomaly, it is important to measure the π^o lifetime as accurately as possible. The present experimental knowledge of the $\pi^o \to \gamma\gamma$ width is summarized in figure 1, along with the projected error of our proposed experiment. Three experimental techniques have been used to measure the neutral pion width: the direct method, $\gamma\gamma$ collisions, and the Primakoff effect.

2.1 The direct method

A direct measurement of the π^o lifetime can be made by observation of the decay distance between the production and decay points. This has proven difficult because of the high spatial resolution which is required due to the short lifetime, $\tau \simeq 10^{-16}$ sec. To be able to discern distinct production and decay points, one must take advantage of relativistic time dilation to have the pion survive long enough in the laboratory frame. Additionally, good knowledge of the energy distribution of the produced pions is necessary in order to extract the lifetime via this method.

The first measurement utilizing such a technique was performed at the CERN PS in 1963 [11]. The precision achieved was 17%. This experiment is not used in the particle data book average. In 1985, an improved version of this technique was employed at the CERN SPS. In this experiment, a 450 GeV/c proton impinged upon two tungsten foils whose separation was variable. The first foil served as the π^o production target, and the second foil converted the π^o decay photons to electron-positron pairs, and the positrons were subsequently detected. For a small foil separation, some of the π^o's decayed after the second foil, whereas for a large separation, essentially all of the π^o's decayed before the second foil. Thus, by measuring the positron rates for three different foil spacings ranging from 5 to 250μm, the authors were able to determine the lifetime. The dominant systematic errors arise from uncertainties in the π^o spectrum which was not measured but was assumed to be the arithmetic mean of the π^+ and π^- spectra. In addition, corrections had to be made for the Dalitz decay of the π^o's, conversion of the photons in the π^o production target, prompt positron and photon production, and positrons from the decay of η's. A pion lifetime of $\tau_{\pi^o} = (0.897 \pm 0.022 \pm 0.017) \times 10^{-16}$ seconds was obtained[13], corresponding to a width of $\Gamma_{\pi^o} = (7.34 \pm 0.18 \pm 0.11)$ eV.

It is interesting to note that this experiment, the most precise of those performed to date, gives a result which is smaller than the leading order chiral anomaly prediction[1, 2]. Furthermore, with the latest next-to-leading calculations described above, the discrepancy between this measurement and theory widens to more than three standard deviations. The experiment proposed here will directly address this discrepancy.

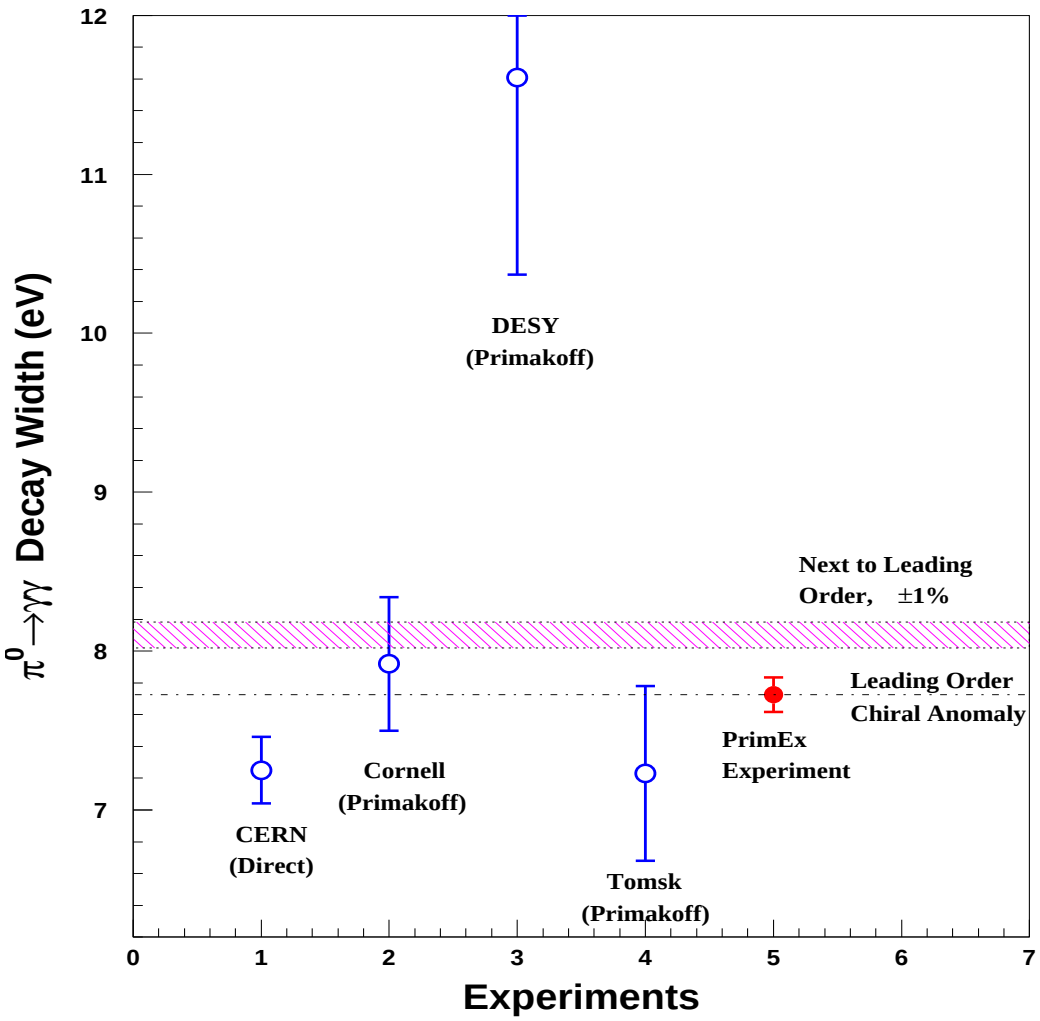

Figure 1: $\pi^o \to \gamma\gamma$ decay width in eV. The dashed horizontal line is the leading order prediction of the axial anomaly (equation 3)[1, 2]. The shaded band is the recent next-to-leading order prediction. The experimental results with errors are for : (1) the direct method[13]; (2,3,4) the Primakoff method [20, 16, 17]; (5) the expected error for the PrimEx experiment, arbitrarily plotted to agree with the leading order prediction.

2.2 Measurements using $\gamma\gamma$ collisions

The π^o width has been measured using electron-positron collisions at DESY via $e^+e^- \rightarrow e^+e^-\gamma^*\gamma^* \rightarrow e^+e^-\pi^o \rightarrow e^+e^-\gamma\gamma$ [12]. The incident leptons are scattered at very small angles and are not detected in the final state. In so doing, they radiate quasi-real photons that couple to the π^o which is subsequently identified in an invariant $\gamma\gamma$ mass spectrum. The photons were detected using the Crystal Ball detector which consists of a large array of NaI(Tl) crystals providing 93% solid angle coverage. Contributions to the systematic error included luminosity normalization, detector efficiencies, cosmic ray rejection, and beam-gas collisions. The latter effect arises from the production of π^o's via the interaction of the leptons with the residual gas in the beam pipe. The resulting width obtained was $\Gamma_{\pi^o} = (7.7 \pm 0.5 \pm 0.5)$ eV, very close to the prediction of the anomaly but with a relatively large error. The value obtained in this experiment is the same as the Particle Data Book average but was not included in this average[3].

2.3 Measurements using the Primakoff effect

The Primakoff effect, *i.e.* photopion production from the Coulomb field of a nucleus[14], has been used in a number of experiments to study the π^o lifetime [20, 16, 17, 18]. The production of π^o's in the Coulomb field of a nucleus by real photons is essentially the inverse of the decay $\pi^o \rightarrow \gamma\gamma$, and the cross section for this process thus provides a measure of the π^o lifetime.

Using bremsstrahlung beams of energy 4.4 GeV and 6.6 GeV at Cornell, Browman *et al.*[20] measured the Primakoff cross sections on several nuclei, and obtained a total decay width of $\Gamma_{\pi^o} = (8.02 \pm 0.42)$ eV. However, as was pointed out in [15, 12] the quoted error, does not have any contribution from uncertainties in the luminosity or detection efficiency (see table 1 of [20]), and is an underestimate. An analogous measurement of the η width[19] using the Primakoff effect employing a very similar setup and analysis procedure is not in agreement with other experiments.

The other two Primakoff measurements shown in figure 1 were performed with bremsstrahlung beams of 1.5 and 2.0 GeV at DESY[16] and 1.1 GeV at Tomsk[17]. From figure 1 it can be seen that the DESY measurement is high compared to the theoretical prediction and the Particle Data Book average. Although both of these measurements have relatively large errors they were included in the Particle Data Book average[3]. An older Primakoff experiment performed with 0.95 and 1.0 GeV bremsstrahlung beams at Frascati[18] has not been included in the Particle Data Book average and is not shown in figure 1.

In view of the strong interest in the subject, the dispersion of the previous results, and the recent availability of high intensity, high energy tagged photon beams, a high precision, state-of-the-art measurement of the π^o lifetime is needed. In particular, the Hall B tagged photon facility at TJNAF will enable a measurement which will offer two distinct advantages over previous measurements involving bremsstrahlung beams: (1) the quasi-monochromatic nature of the tagged beam will enable a clean kinematical separation of the Primakoff mechanism from various background processes, and (2) the tagging technique will enable significantly better control of systematic errors associated with the photon flux normalization.

3 Overview of the Experiment

We plan to use the quasi-monochromatic photons of energy 4.6-5.7 GeV from the Hall B photon tagging facility to measure the absolute cross section of small angle π^o photoproduction from the Coulomb field of complex nuclei. The invariant mass and angle of the pion will be reconstructed by detecting the π^o decay photons from the $\pi^o \rightarrow \gamma\gamma$ reaction.

For unpolarized photons, the Primakoff cross section is given by[16]:

$$\frac{d^3\sigma_P}{d\Omega} = \Gamma_{\gamma\gamma}\frac{8\alpha Z^2}{m^3}\frac{\beta^3 E^4}{Q^4}|F_{e.m.}(Q)|^2 sin^2\theta_\pi \tag{4}$$

where $\Gamma_{\gamma\gamma}$ is the pion decay width, Z is the atomic number, m, β, θ_π are the mass, velocity and production angle of the pion, E is the energy of incoming photon, Q is the momentum transfer to the nucleus, and $F_{e.m.}(Q)$ is the nuclear electromagnetic form factor, corrected for final state interactions of the outgoing pion.

As the Primakoff effect is not the only mechanism for pion photoproduction at high energies, some care must be taken to isolate it from competing processes. In particular, the full cross section is given by:

$$\frac{d^3\sigma}{d\Omega_\pi} = \frac{d\sigma_P}{d\Omega} + \frac{d\sigma_C}{d\Omega} + \frac{d\sigma_I}{d\Omega} + 2\cdot\sqrt{\frac{d\sigma_P}{d\Omega}\cdot\frac{d\sigma_C}{d\Omega}}cos(\phi_1+\phi_2) \tag{5}$$

where the Primakoff cross section, $\frac{d\sigma_P}{d\Omega}$, is given by equation (4). The nuclear coherent cross section is given by:

$$\frac{d\sigma_C}{d\Omega} = C\cdot A^2|F_N(Q)|^2 sin^2\theta_\pi \tag{6}$$

and the incoherent cross section is:

$$\frac{d\sigma_I}{d\Omega} = \xi A(1-G(Q))\frac{d\sigma_H}{d\Omega} \tag{7}$$

where A is the nucleon number, $Csin^2\theta_\pi$ is the square of the isospin and spin independent part of the neutral meson photoproduction amplitude on a single nucleon, $|F_N(Q)|$ is the form factor for the nuclear matter distribution in the nucleus, (corrected for final state interactions of the outgoing pion), ξ is the absorption factor of the incoherently produced pions, $1-G(Q)$ is a factor which reduces the cross section at small momentum transfer due to the Pauli exclusion principle, and $\frac{d\sigma_H}{d\Omega}$ is the π^o photoproduction cross section on a single nucleon. The relative phase between the Primakoff and nuclear coherent amplitudes without final state interactions is given by ϕ_1, and the phase shift of the outgoing pion due to final state interactions is given by ϕ_2.

Kinematical considerations enable one to separate the Primakoff effect from other photo-pion production mechanisms. The Primakoff cross section is zero for pions emitted along the incident photon direction, has a sharp maximum at an angle $\theta_\pi \sim m_\pi^2/2E_\pi^2$, and falls rapidly to zero at larger angles. It is proportional to Z^2, and its peak value is roughly proportional to E^4. The nuclear coherent cross section for spin zero nuclei is also zero in the forward direction, but has a broad maximum outside the angular region of the Primakoff effect, and falls at larger angles as shown in figure 2, where the amplitudes are normalized to the Cornell

data[20], and distortion effects are included. It is expected to vary little with energy[16]. Measurements of the nuclear effects at larger angles are necessary to determine the unknown parameters in the production mechanism and thus make an empirical determination of the nuclear contribution in the Primakoff peak region. Consequently, this experiment requires a π^o detector with good angular resolution to eliminate nuclear coherent production, and good energy resolution in the decay photon detection will enable an invariant mass cut to suppress multi-photon backgrounds.

We are planning to take extensive data to test the experimental accuracy of the proposed measurements. These are based on the fact that the production of neutral pions via the Primakoff effect is primarily an electromagnetic phenomenon and, therefore, can be accurately calculated. The main features of the Primakoff effect (listed above) will be used to test the accuracy of our data: (1) We will take data with sufficient angular resolution to check the shape of the Primakoff peak after the coherent nuclear and nuclear-Primakoff interference amplitudes, which will be determined empirically by larger angle data, have been subtracted; (2) three spin zero targets (^{12}C, ^{120}Sn, ^{208}Pb) will be used. These have form factors which have been well studied by electron scattering experiments, and can be used to test the Z^2 dependence of the cross section; and (3) the E^4 dependence of the peak cross section will be measured in the energy range from 4.6 to 5.7 GeV. The study of the Primakoff peak as a function of these three variables should add a great deal of confidence to the measurement, and can be used to empirically determine the systematic errors.

4 Accomplishments and Technical Readiness

The primary experimental equipment required in this experiment includes: (1) the Hall B photon tagger; (2) 5% radiation length solid π^o production targets (^{12}C, ^{120}Sn, and ^{208}Pb); (3) a pair production luminosity monitor located just downstream of the π^o production target; (4) a 1m $\times$ 1m highly segmented lead glass photon detector for π^o decay photons with a high resolution insertion in the central region near the beam, and a plastic scintillator charged particle veto. (See figure 3.) Here, we describe the progress made in preparation for this experiment.

4.1 Funding and Contributions of Major Capital Equipment

In August of 2000, $1 million from the Major Research Instrumentation (MRI) program of the National Science Foundation was awarded for the development of experimental apparatus for this experiment (award number PHY-0079840). The details of this funding request can be found in the *PrimEx Conceptual Design Report*[21] in which we argued that the apparatus necessary for this experiment will also enhance the present Hall B experimental program as well as enable future experiments. Subsequently, Jefferson Lab has provided significant infrastructure as well as technical and engineering support for these efforts. Major contributions provided by Jefferson Lab have included support for Russian members of the PrimEx Collaboration, approximately $100k for the PrimEx Hybrid Calorimeter frame and remote control, and approximately $100k for the power supply for the PrimEx/Hall B pair spectrometer magnet. The Collaboration has also sought out and obtained equipment

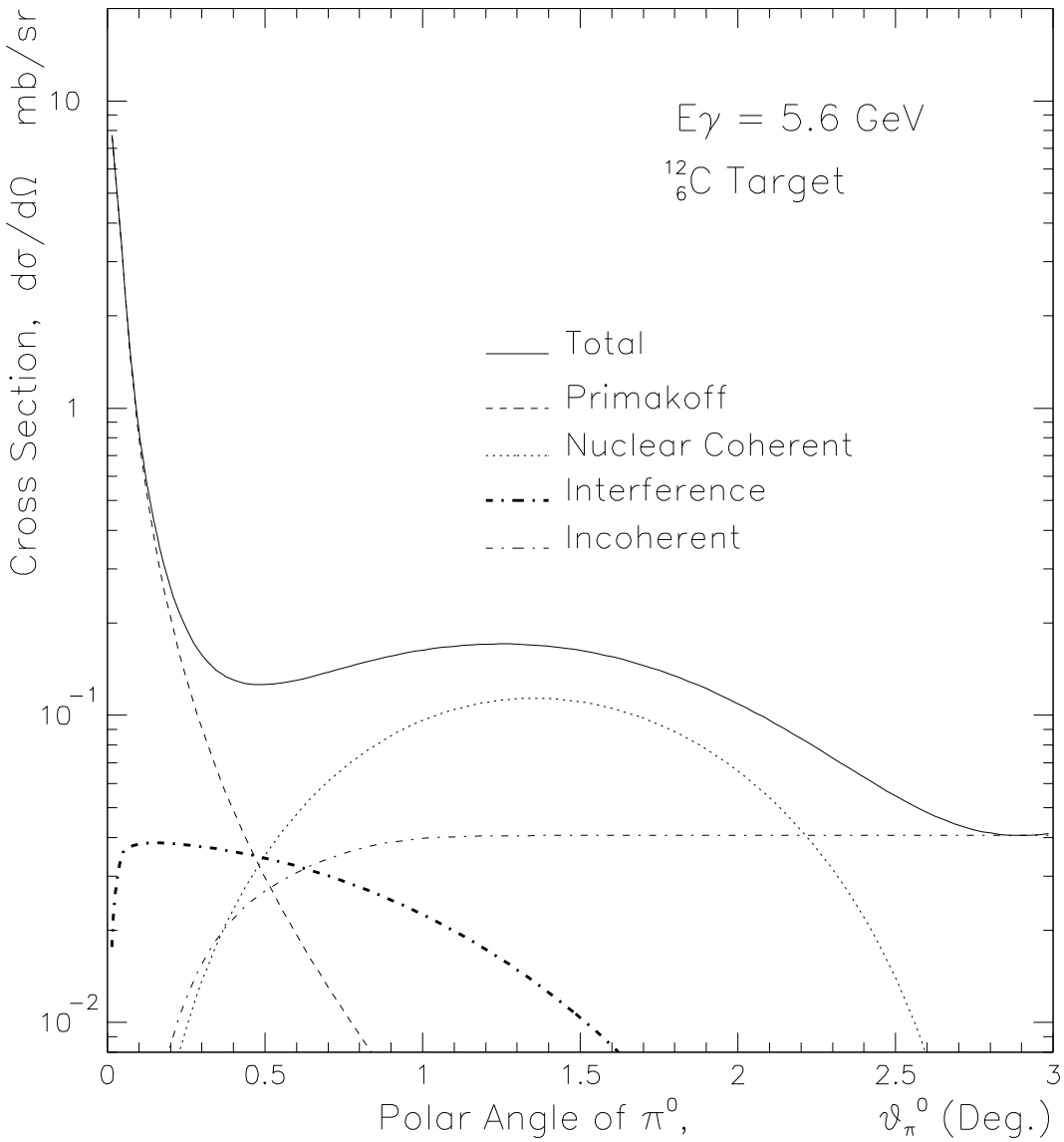

Figure 2: Angular behavior of the electromagnetic and nuclear π^o photoproduction cross sections for ^{12}C in the 6.0 GeV energy range.

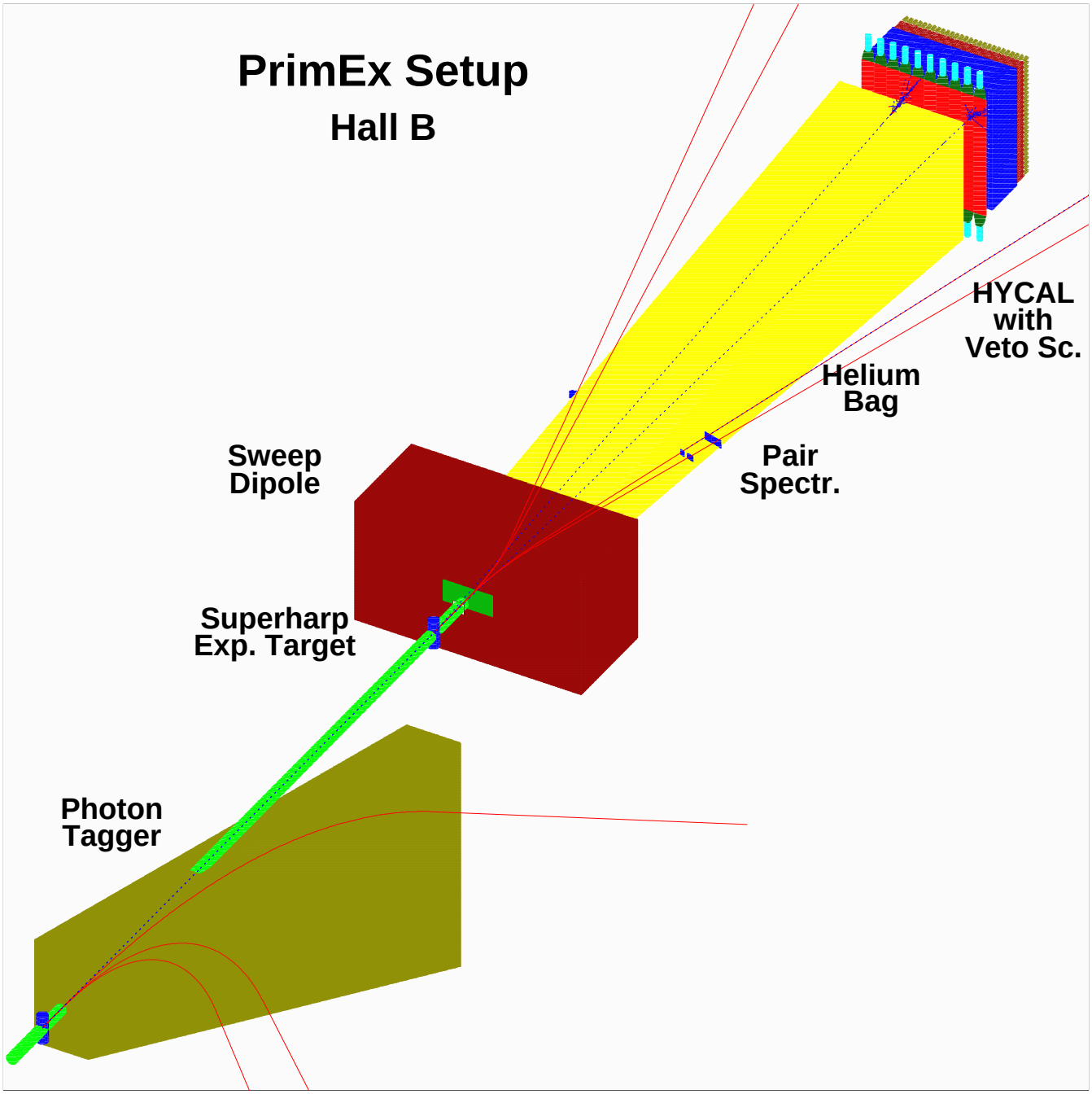

Figure 3: Layout of the experimental setup.

from other DOE laboratories. The PrimEx/Hall B pair spectrometer dipole magnet is on loan from Brookhaven National Laboratory, and FermiLab has provided data acquisition electronics including 1500 ADC channels (LeCroy1881M modules), two Fastbus crates with power supplies, and numerous cables. We have also obtained 1000 lead glass blocks from the Institute for Theoretical and Experimental Physics in Moscow, Russia, and an additional 1000 lead glass blocks from the Institute for High Energy Physics in Protvino, Russia. The recent availability of low cost, high quality lead tungstate scintillation crystals from China has enabled the central high resolution region of the Hybrid Calorimeter to be enlarged. As such, the calorimeter currently under construction is expected to be superior in performance to that envisioned in the original proposal. At present, approximately 75% of the funds allocated for this project have been spent for research and development and procurement of equipment.

4.2 Beamline Instrumentation

4.2.1 The Total Absorption Counter for Flux Monitoring

Since each π^o decay event is measured in coincidence with a counter in the Hall B photon tagger, the normalization of the cross section to the incident photon flux depends on knowing the number of tagged photons on target in each energy bin during the run. The number of tagged photons on target is not necessarily equal to the number of events recorded by the tagging counters because of a number of effects:

(1) events in which a bremsstrahlung photon is produced but is absorbed before reaching the target.

(2) Møller scattering events in the bremsstrahlung radiator which produce an electron in the tagging counters without an accompanying photon.

(3) Extra electrons registered due to room background.

Events of the first type will be minimized by allowing the entire bremsstrahlung beam to travel in vacuum without collimation to the target. The second category of events is known to affect the tagging rate at the level of a few percent. The combination of these first two effects can be measured by performing a calibration run in which the Primakoff target is removed and a lead glass total absorption counter (TAC) is placed in the photon beam just after the vacuum window downstream of the Primakoff target position. The ratio of Tagger·TAC coincidences to tagger events, the so called tagging efficiency, is then recorded. Knowing this ratio, one can determine the tagged photon flux in the data taking run by counting the number of post bremsstrahlung electrons in a given tagging counter:

$$N_\gamma^{tagged}(experiment) = N_e(experiment) \times \frac{N_\gamma^{tagged}(calibration)}{N_e(calibration)} \tag{8}$$

One can then determine the cross section from the tagged yield of π^o's:

$$\text{TaggedYield} = \frac{d\sigma}{d\Omega} \times t \times \Delta\Omega \times N_e(experiment) \times \frac{N_\gamma^{tagged}(calibration)}{N_e(calibration)}, \tag{9}$$

where t is the target thickness, and $\Delta\Omega$ is the solid angle of the pion detector. In the calibration run, the total absorption counter rate is limited, and, therefore, the tagging efficiency must be measured at a rate which is reduced by a factor of about one hundred as compared to the data taking run.

For these measurements, the Hall B total absorption counter has been upgraded by the PrimEx Collaboration. It is presently a single lead glass block (SF-5), with dimensions $20cm \times 20cm$ transverse to the beam and $40cm$ long. It is viewed by a single five inch diameter Hamamatsu photomultiplier. Initial commissioning of this detector was performed in September of 2001.

4.2.2 Harp

A harp is located in front of the Primakoff production target in order to monitor the photon beam profile and position. This consists of a relatively thick wire which moves through the photon beam. Secondary particles which are subsequently produced in the wire are detected downstream using the pair spectrometer system which is described in more detail below. The main components of the harp are: a fork with two tungsten wires, a stepper motor with an accuracy of motion of about $10\mu m$, an encoder, and a particle detector consisting of the scintillator telescopes of the luminosity monitor run in either coincidence or singles mode. The fork is positioned at 45° with respect to the horizontal and moves in the plane perpendicular to the beamline. The distance between the two arms of the fork is 1 inch. Two wires are positioned between the arms in such a way that the first wire is vertical and moves in the horizontal direction across the beam, and the second wire is horizontal and moves in the vertical direction when the fork advances into the beam. When the wire crosses the beam, beam particles scatter from the wire or produce e^+e^- pairs, which are analyzed in the magnetic field of the pair spectrometer dipole and detected in the scintillator telescopes. Using the information from the encoder, one can construct a scanning plot which represents the number of counts *versus* the wire position. This plot provides the vertical and horizontal beam profiles.

4.3 PrimEx Targets

Three experimental targets will be employed in the PrimEx experiment – ^{12}C, ^{120}Sn, and ^{208}Pb – each 5% of a radiation length in thickness. In the Primakoff process the reaction mechanism is simplified if the target nucleus has $J^\pi = 0^+$. Therefore, isotopically enriched materials are required for the tin and lead targets. The ^{120}Sn and ^{208}Pb targets were ordered from Oak Ridge National Laboratory at a cost of approximately $12.5k and delivered in early summer of 2001. The enrichments are 98.29% for the tin target, and 99.09% for the lead target.

In this experiment, we require that the target thickness, ρ_t, be known to a precision better than $\pm 0.7\%$. In principle this tolerance can be satisfied by micrometer measurements with an accuracy of ± 0.05 mil, and micrometers of this accuracy are commercially available. However, use of a micrometer could produce indentations or bends in the metal foils. For this reason we plan to perform direct measurements of the metal foils with a technique that avoids direct contact with the target. X-ray attenuation represents the basis for such a

determination. In this technique a line source of X-rays is collimated to a spot size a few mm in diameter and detected in a NaI detector behind the target foil. For these measurements we use the 60 keV X-ray line from ^{241}Am. The attenuated X-ray intensity through the foil is given by:

$$I(T) = I_0 B(T) e^{-T/\lambda}$$

where I_0 is the unattenuated intensity, T is the target thickness, λ is the X-ray attenuation length, and B(T) is the buildup factor. Provided that λ and the functional dependence of the buildup factor on T are known, T can be obtained from a measurement of the attenuated X-ray flux through the target foil.

Purely exponential attenuation, where the buildup factor B(T) is unity, is only realized in a situation where the X-ray collimation is perfect and the X-ray detector subtends zero solid angle. In more realistic situations, Compton scattering in the target foil leads to non-exponential attenuation. Using 60 keV X-rays and tin and lead foils of approximately 5% radiation lengths in thickness, we found that the buildup factor can be empirically parameterized by

$$B(T) = 1 + bT/\lambda$$

where b is a constant, approximately 0.07 for tin, and 0.15 for lead. Therefore, the flux decreases more slowly with increasing foil thickness than for pure exponential behavior. We found no evidence that higher order terms in T/λ play a significant role in the buildup factor for 5% radiation length targets.

To calibrate the measurements, we plan to first make a micrometer measurement at one point on the target and then to X-ray that point. This provides a calibration for the parameter b. The X-ray attenuation lengths are known with sufficient accuracy at 60 keV for tin and lead, at about the 1% level, and can be taken from the literature. Then other points of the target are X-rayed and the target thickness obtained from the attenuated X-ray flux. We plan to take a micrometer measurement on at least one other point of the target to cross calibrate the procedure.

The targets will be scanned over the X-ray source to obtain a map of ρ_t as a function of x and y. Scanning a thick high-Z wire through the beam fiducializes the position of the X-ray beam. In this case we look for a dip in the count rate as the wire passes through the X-ray beam.

The X-ray scan apparatus has been designed and constructed and is controlled by LabView. A 1" NaI crystal is used to the detect X-rays and the NaI pulse height is readout through a CAMAC ADC system, also running under LabView control. We plan to complete thickness measurements of the tin and lead targets in the Summer of 2002.

The carbon target will be machined from a block of pyrolytic graphite (PG) of natural isotopic purity. PG is a crystalline form of graphite that is produced using high temperature Chemical Vapor Deposition furnace technology. The low porosity of PG, approximately 1%, as compared to 10% for normal graphite makes it an ideal material for use as a target. The PG density depends somewhat on the specifics of the manufacturing process. However, PG densities are typically close to the theoretical limit of 2.25 g/cm^3. We plan to measure the density of the PG target in a specific gravity setup using an electronic scale and ultrapure

water. Laboratory tests have indicated that we can achieve the required level of precision for the density. The thickness of the target (approximately 1 cm) will be measured with a micrometer; a prototype target machined from a block of normal graphite had thickness variations of approximately 0.1%. Finally, as a last check on ρ_t, we plan to X-ray the carbon target to make sure there are no internal voids in the PG material.

We have obtained a sample of PG from SLAC that is sufficiently large that several targets can be cut from it. A target has been successfully machined from the sample, which will be used in our measurement studies in the summer of 2002.

The PrimEx target ladder and moving mechanism have been designed, constructed and assembled by the JLab technical staff. The target ladder can move in both the horizontal and vertical directions, giving us fine control over exactly where we place the photon spot on the target. There are positions on the target ladder for six targets – the three production targets, a blank, a crossed wire to fiducialize the position of the photon beam by use of pair production, and a thin foil to be used in tests of the pair spectrometer. For the September 2001 test run we had the target x-motion instrumented under EPICs control. Slow-controls for both the x and y motion will be complete in the Summer of 2002.

4.4 The PrimEx/Hall B Pair Spectrometer

The use of the total absorption counter to calibrate the number of photons per tagging electron will provide an absolute calibration of the photon flux incident on the π^o production target. However, these measurements will be performed at intervals throughout the data taking, and will by necessity be performed at an electron beam current which is two orders of magnitude less than the production data taking runs. Consequently, we have constructed a pair production luminosity monitor which will measure the relative tagged photon flux over a range of intensities, and will operate continuously throughout the data taking runs.

The pair spectrometer will use the physics target as a converter, and will make use of the 15 kgauss-meter dipole magnet placed just downstream of it. The electrons and positrons are detected on either side of the beam in a series of plastic scintillator telescopes. The requirements of the pair spectrometer are that it must operate over the entire range of intensities (of both the flux calibration and data taking runs) and have a smooth, relatively flat acceptance in E_γ covering the entire tagging range. The segmentation of the pair spectrometer detectors is driven by the fact that the pair production and Primakoff target are the same, and therefore the pair spectrometer detectors must accommodate the rates from a 5% radiation length target. Under the PrimEx run conditions, we expect singles rates on a single telescope to be about 140kHz, and a total of 90kHz of pair spectrometer-tagger coincidences over the range of tagging energies from $0.77E_o$ to $0.95E_o$. The efficiency of the pair spectrometer for tagging photons will be about 0.6%. A schematic of the pair spectrometer with one simulated pair production event is shown in figure 4. Each arm presently consists of eight telescopes with overlapping momentum acceptances placed symmetrically on either side of the beamline. We are currently in the process of upgrading this to 16 telescopes on each side (for a total of 64 detectors) to provide the ability to tag photons over nearly the entire range of the Hall B tagger, from $0.2E_o$ to $0.95E_o$.

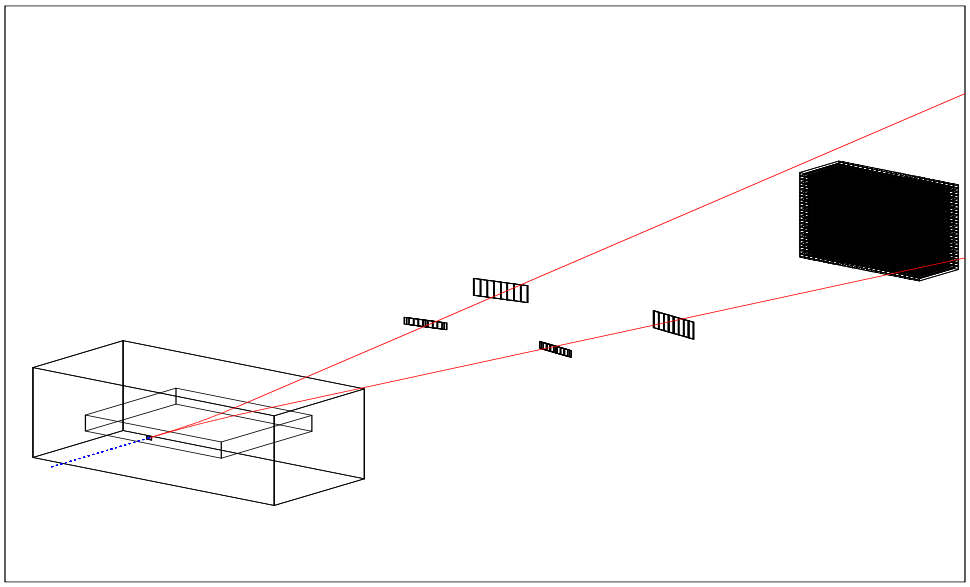

Figure 4: Layout of the luminosity monitor and one pair production event. Each detector arm is currently segmented into eight contiguous plastic scintillator telescopes.

4.4.1 Dipole and Vacuum Box

The dipole magnet for the PrimEx/Hall B pair spectrometer is on loan from Brookhaven National Laboratory and its associated power supply was purchased by Jefferson Lab. The magnet has been refurbished, installed in the Hall B beamline, and commissioned. The vacuum box for the pair spectrometer was constructed at Arizona State University and delivered to Jefferson Lab in January 2001. It is currently installed on the beamline.

4.4.2 Results from Magnet Mapping

The PrimEx/Hall B pair spectrometer magnet was mapped in Hall B with the vacuum box in place in May 2001. The mapping system consisted of three Hall probes, one on the median plane of the magnet and one each at 2 centimeters above and below the median plane. A picture of the apparatus is shown in figure 5.

The principal achievements of these measurements are:

- The procedure to set up the field was established.
- The excitation curve (central field *versus* current) was measured with an NMR probe.
- Full maps were obtained at 0.5, 0.9, 1.0, 1.3, 1.5, and 1.6 Tesla.
- Central line fields were measured from 0.2 to 1.8 Tesla in 0.2 T steps.

The $\int Bdl$ was determined to better than 0.1%. An example of one such map is shown in figure 6, which was obtained at a central field of 1 Tesla.

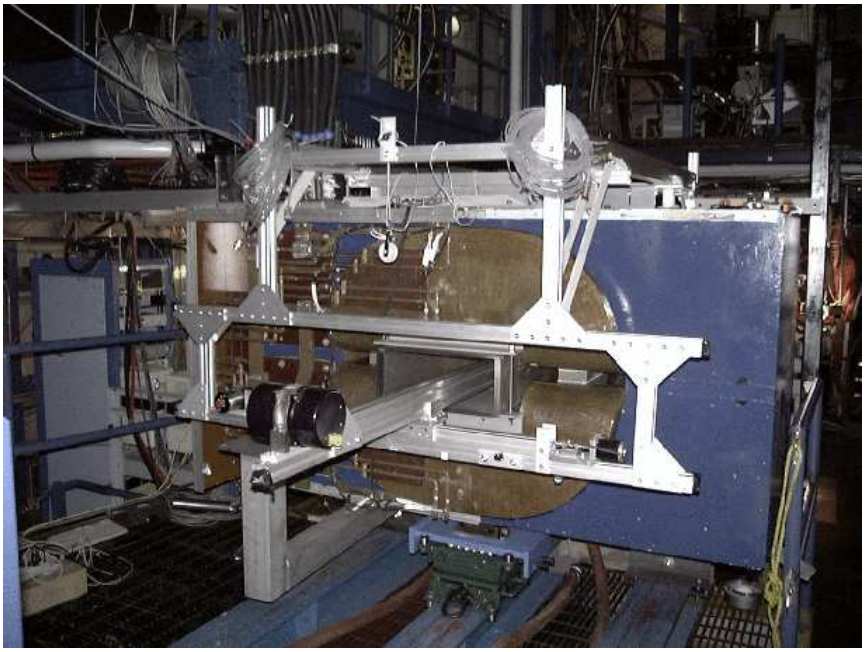

Figure 5: The PrimEx/Hall B pair spectrometer being mapped in the Hall. View is from the upstream side of the magnet looking downstream

4.4.3 Detectors

The full complement of pair spectrometer detectors required for the PrimEx run (16 telescopes or a total of 32 detectors) is constructed and installed in the Hall. For general use to the Hall B photon physics program, we are presently constructing an additional 16 telescopes to extend the range of photon energies which may be tagged.

Figure 7 shows a side view of a detector module. The front scintillators are $2.4cm \times 7.5cm$ and $0.5cm$ thick, and the rear scintillators are $9.3cm \times 3.1cm$ and $2cm$ thick. The photomultiplier tubes (front detectors: Hamamatsu R6427, rear detectors: R580-17) are shielded from magnetic fields with μ metal, and their voltage dividers have been modified to enable extra power supplies to be applied to the last three dynodes for enhanced high rate capability.

A drawing of the detector assembly is shown in figure 8. The detector mounting system has been designed so as not to interfere with the geometrical acceptance of the HYCAL which is downstream of it, and the amount of material in the median plane of the magnet has been minimized using carbon composite material. A photograph of the detectors and support frame in the Hall is shown in figure 9.

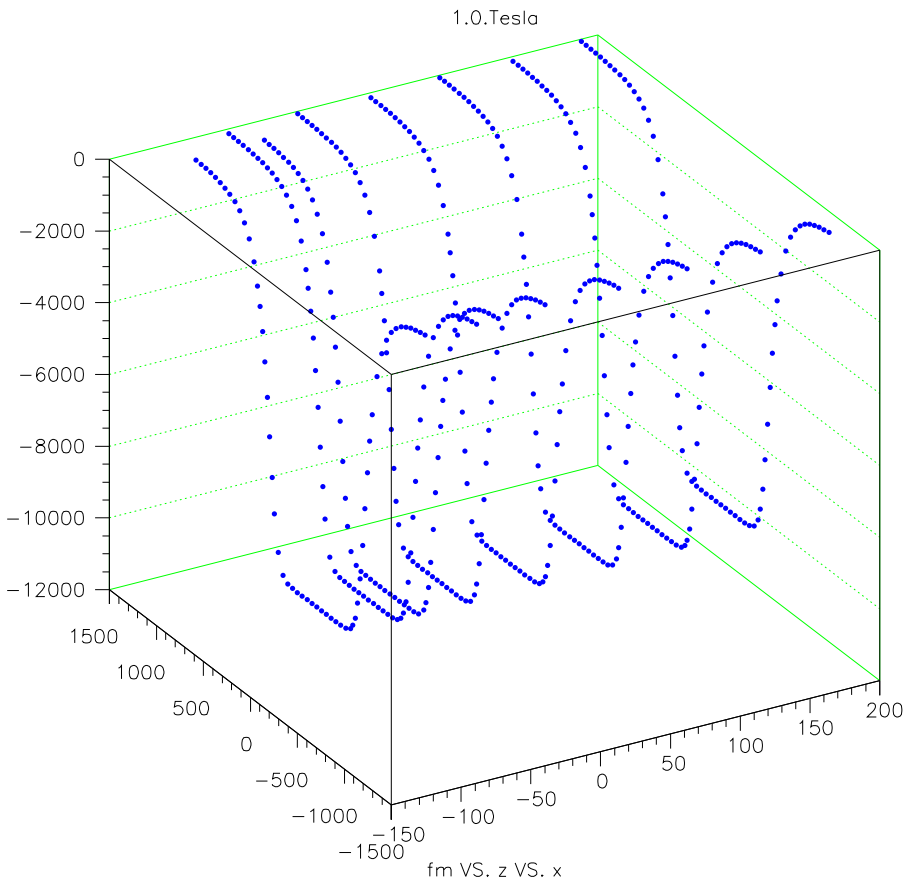

Figure 6: Field map of the PrimEx/Hall B pair spectrometer dipole at a central field of 1 Tesla.

The pair spectrometer and its associated data acquisition electronics has been installed, and is currently being commissioned. Preliminary commissioning was done during the $g8$ run in the summer of 2001, and partial commissioning was done in mid-September of 2001. A typical online plateau curve for a detector module, taken with beam, showing singles rates *versus* high voltage is shown in figure 10.

4.5 The Hybrid Calorimeter - HYCAL

At the incident photon energies of this experiment ($E_\gamma = 4.6 - 5.7$ GeV), the Primakoff cross section peaks at extremely small angles. For instance at $E_\gamma = 5$ GeV, $\theta_{peak} = 0.02^o$. In order to identify and extract the Primakoff amplitude, the experimental setup must have sufficient angular resolution for forward pion production. Both photons from the $\pi^o \rightarrow \gamma\gamma$ decay will be detected in the electromagnetic hybrid calorimeter (HYCAL). Therefore the pion angular resolution will depend strongly on the position and energy measurement accuracy of the calorimeter. Implementation of the photon tagging technique will, in addition to photon flux control, provide information on the initial photon energy at the level of 10^{-3}. This knowledge of the initial photon energy will apply a kinematical constraint to this two body reaction and result in about a 30% improvement in the angular resolution[21]. We are constructing

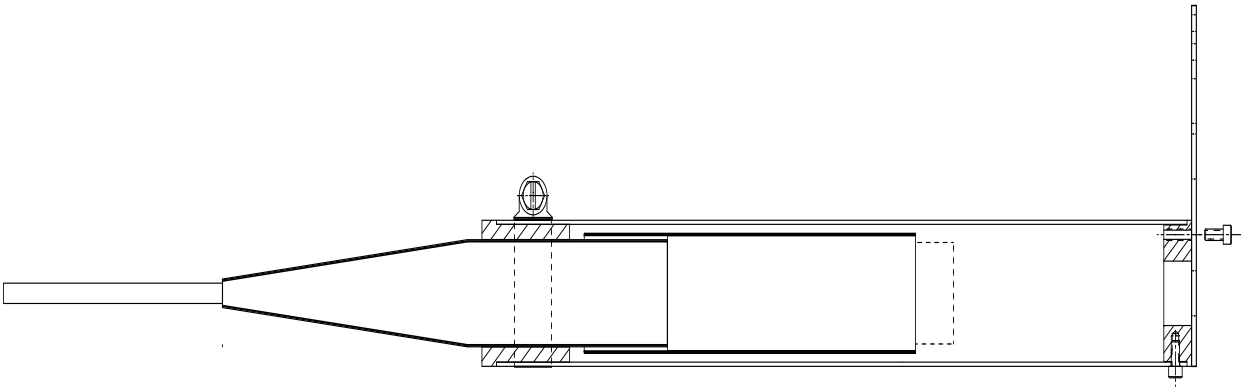

Figure 7: Side view of a front detector module. Scintillator (left, viewed edge-on), light guide (center), and photomultiplier tube (right) are all glued with optical cement. Patch panel for routing cables extends upward on the right.

a multichannel hybrid calorimeter which will consist of two types of shower detectors: lead glass Cherenkov modules located on the peripheral part of the calorimeter, and lead tungstate scintillating crystals in the central region with a hole in the middle for the passage of the photon beam through the calorimeter. This design is based on an optimization of the cost and performance of the calorimeter. The $PbWO_4$ crystals are half the size of the lead glass Cherenkov radiators, and provide energy and position resolutions which are approximately twice better. On the other hand, the price per unit area of detector is approximately 4-5 times higher for the crystal detectors as compared to lead glass. The transverse dimensions of the HYCAL calorimeter (116 x 116cm^2) were chosen to have sufficient geometrical efficiency with the fixed central hole ($4\times4cm^2$) in the middle of the detector. At a distance of 7.5 m from the production target, the designed setup has about a 70% geometrical acceptance for the forward going neutral pions.

During the past two years of research and development work on the $PbWO_4$ detectors, we performed two beam tests for the prototype detectors including crystals from the two major manufacturers – Bogoroditsk Techno-Chemical Plant (BTCP), Bogoroditsk, Russia and the Shanghai Institute of Ceramics (SIC), Shanghai, China. In addition, we have performed studies of their mechanical and optical properties. Figure 11 shows the transmission as a function of wavelength, measured at Jefferson Lab, for two types of crystals. The energy and position resolutions as well as the effect of the rate dependence of the light yield for both types of crystals for a few GeV electron beam were also measured. The results of these tests are described below. We chose to purchase the crystals from SIC based on the high performance they exhibited in these tests as well as the comparatively lower price which we were able to obtain through our Chinese collaborators. This has enabled us to increase the number of crystals in the calorimeter by more than a factor of two and thereby enhance its high resolution capabilities. The final design for the HYCAL will consist of 1152 $PbWO_4$ crystals which will cover the 70×70 cm^2 central part of the calorimeter. At present, we have onsite at JLab 800 lead tungstate crystals. The remaining 450 will arrive in early July 2002. The rest of the calorimeter is being instrumented with the 576 lead glass Cherenkov counters.

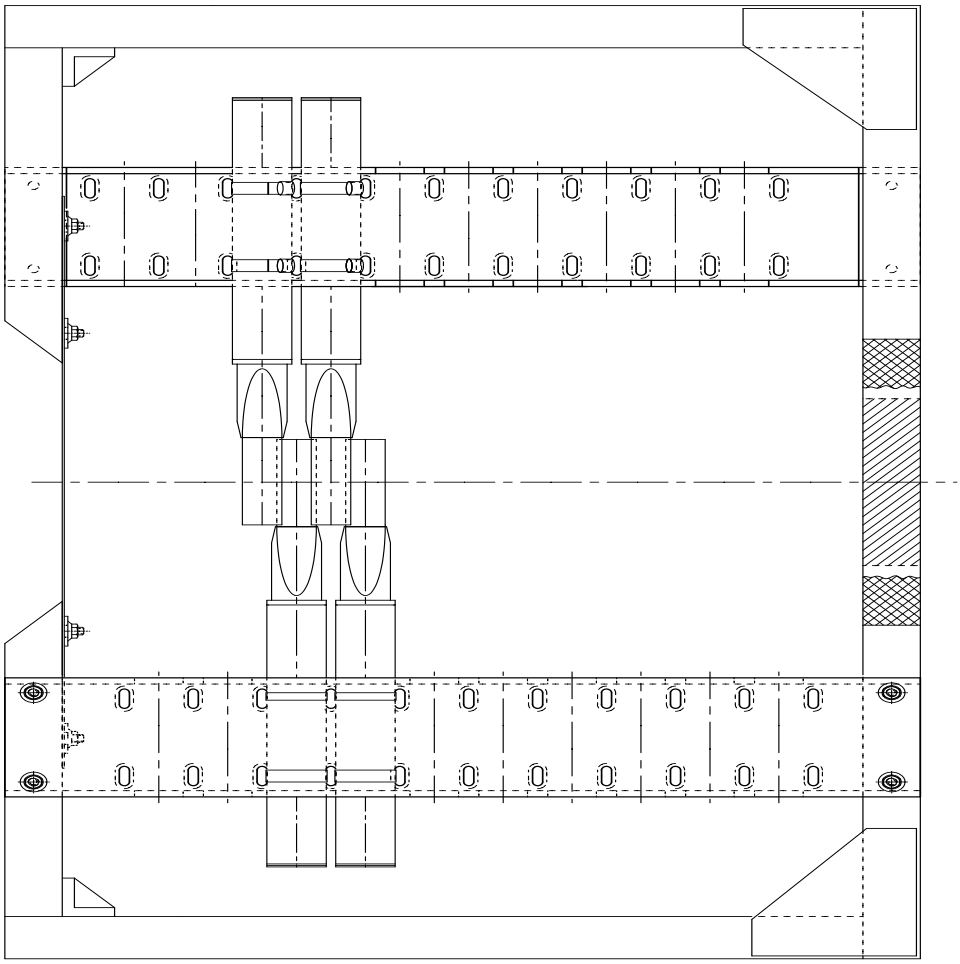

Figure 8: The pair spectrometer detector support frame, with four detectors shown mounted.

During data taking, the calorimeter will be calibrated with tagged photon beams to determine the gains of the counters. For this purpose, the calorimeter will be installed on a transporter allowing every counter of the detector to be centered on the beam. To monitor and correct possible gain changes between beam calibrations, a light monitoring system will be used which is described separately in section 4.5.7.

4.5.1 Lead Glass Detectors

Two institutions from Russia which have provided lead glass detectors for the HYCAL calorimeter are involved in the collaboration–the Institute for Theoretical and Experimental Physics (ITEP), Moscow and the Institute for High Energy Physics (IHEP), Protvino. In the past three years, we have done several beam tests to define the best lead glass detectors for this experiment. The main considerations have been to optimize the detection efficiency as well as the energy and position resolutions for few GeV photons. The latest lead glass prototype detector is shown in figure 12. The results for the energy and position resolution in the few GeV range are shown in figures 13 and 14. Based on these test results, we have selected TF-1 type lead glass modules with dimensions $3.8\times3.8\times45cm^3$. Our Russian

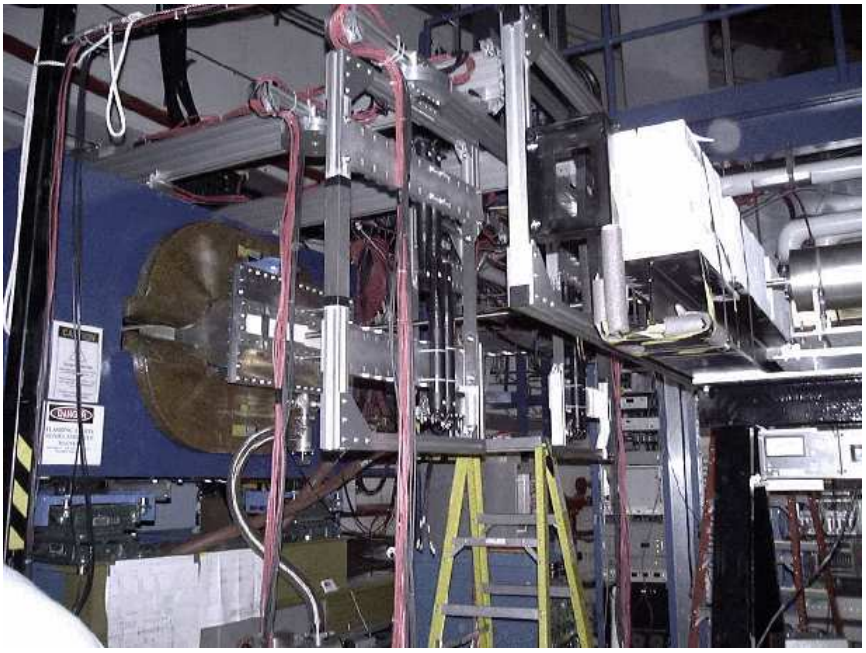

Figure 9: Pair spectrometer detectors and support frame being installed. The downstream side of the PrimEx/Hall B pair spectrometer magnet is on the left.

collaborators have already delivered to Jefferson Lab 1000 modules of lead glass radiators along with a similar amount of photomultiplier tubes and high voltage dividers for HYCAL construction.

The main requirement for the mechanical construction of the lead glass counters has been to make them *"stand alone"* detectors in order for them to be separately tested and assembled in the support frame. The design work for the lead glass counters is complete, and all parts for the mechanical assembly are ordered. We have started mass production of these counters at Jefferson Lab. In figure 15, a fully assembled lead glass counter is shown. Cherenkov light produced in the lead glass radiator from the electromagnetic shower will be detected by a photomultiplier tube (FEU-84-3, made in Russia). The individual blocks are wrapped in $25\mu m$ aluminized mylar foil which serves as a light reflector and an optical isolator between the blocks. The mechanical assembly of each module consists of two brass flanges which are kept together by $25\mu m$ thick stressed brass strips.

We presently have 100 fully assembled counters which will be used for the HYCAL prototype detector beam tests this June (2002). We will have assembled all 650 lead glass counters by September 2002. Final assembly of these detectors in the HYCAL frame will

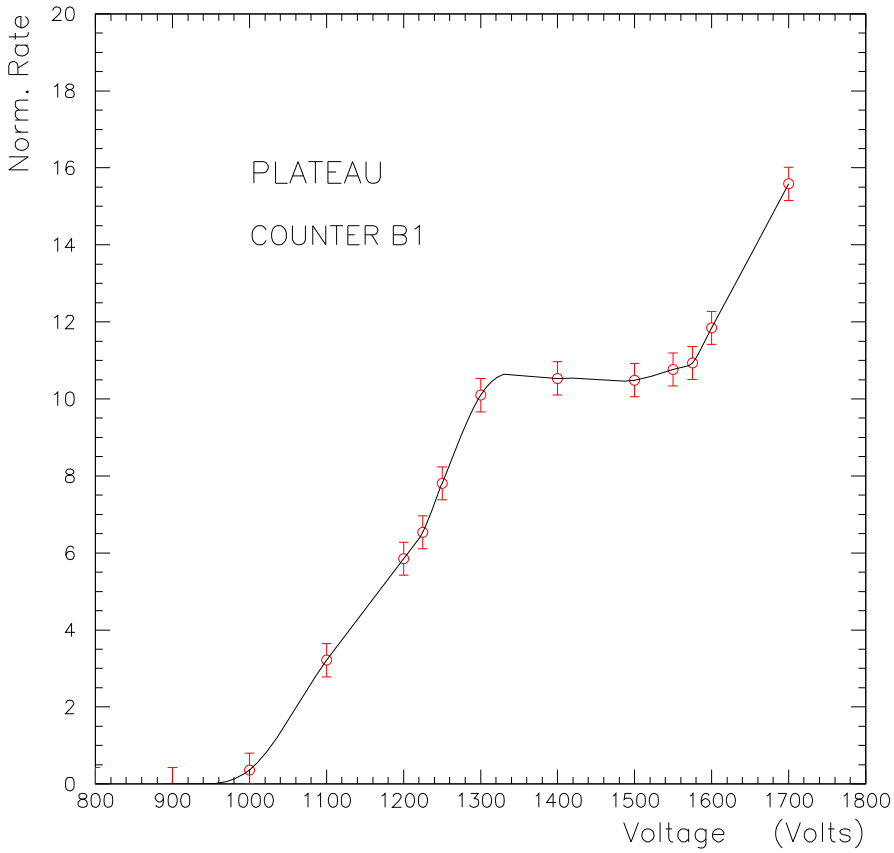

Figure 10: Typical online high voltage plateau curve for a pair spectrometer detector.

occur this Fall in the Test Lab. Cosmic ray tests will be performed before the commissioning of the HYCAL calorimeter in the Hall B photon beam.

4.5.2 Beam Test Results for the Lead Tungstate Detectors

Because of its fast decay time, high density, and high radiation hardness, lead tungstate ($PbWO_4$) has become a popular inorganic scintillator material for precision compact electromagnetic calorimeters in high energy physics experiments (CMS, ALICE for LHC) in the past decade. There are two major commercial suppliers of $PbWO_4$ crystals: the BTCP factory in Bogoroditsk, Russia, and SIC, in Shanghai, China. In order to check the performance of the crystals with few GeV electron/photon beams and also to select the manufacturer for the HYCAL calorimeter, we have done two beam tests with a prototype crystal detector. A matrix consisting of 6×6 $PbWO_4$ crystals was stacked in a light tight aluminum frame which could be cooled down to a well stabilized temperature (T = $4°C$ for these tests). The latest prototype detector is shown in figure 16, viewed from the front-top after removal of the front cover. The light yield of the crystal is highly temperature dependent ($\sim 2\%/^oC$ at room temperature). Therefore one of the technical challenges for this detector is to reach high stabilization of the crystal temperature during the experiment. In order to accomplish this, the crystal assembly was surrounded by massive copper plates (see figure 16) with water

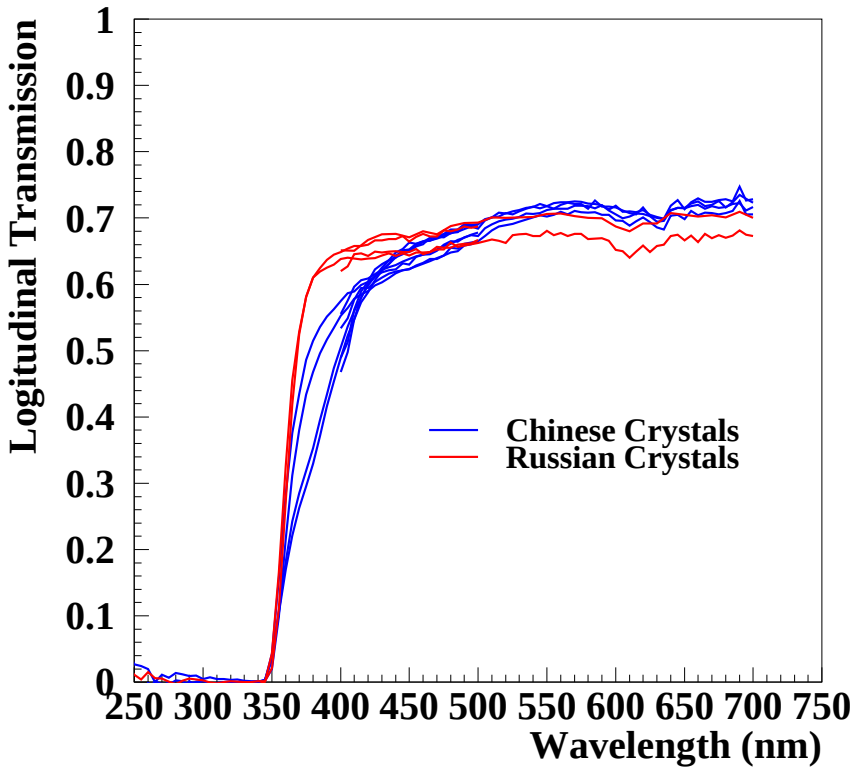

Figure 11: Transmission as a function of wavelength for lead tungstate crystals.

circulating through pipes. Six of the crystals were equipped with temperature sensors on their front faces and read out by computer during the beam test measurements. In figure 17, we show the temperature stability for several crystals during twelve hours of data taking in a tagged photon beam. As can be seen from the plot, the temperature in the prototype calorimeter was stabilized at the level of $\pm 0.1°C$.

The upper 3×6 section of the detector was assembled from crystals made in Russia, and the bottom section consists of Chinese crystals from SIC. The scintillation light from the electromagnetic shower was detected with Hamamatsu R4125HA photomultiplier tubes coupled to the back of the crystals with optical grease. Individual crystals were wrapped in $100\mu m$ TYVEK. The photomultiplier tubes were attached to the crystals with two specially designed brass flanges attached to the front and back of the crystals. These brass pieces are kept together by two stretched $25\mu m$ thick brass strips as can be seen in figure 18.

We moved the prototype detector by remote control in two dimensions perpendicular to the secondary electrons, which were selected by the PrimEx/Hall B dipole magnet and the scintillating telescopes. A x and y coordinate scintillation fiber detector (2 mm in fiber size) was used on the front of the detector to define the impact points of the electrons. The anode output from each photomultiplier tube was digitized by means of a 14-bit charge-

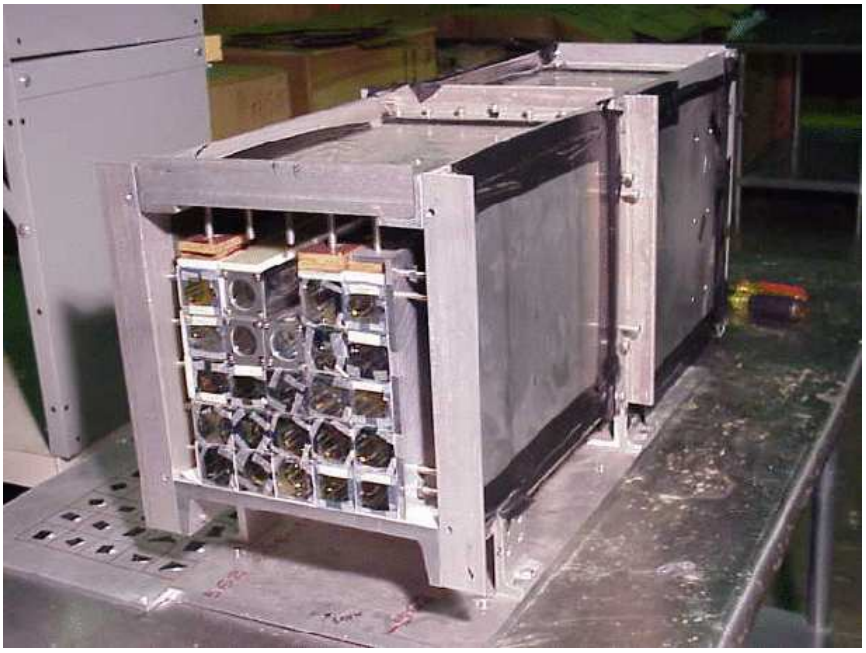

Figure 12: The prototype lead glass detector.

sensitive ADC (LeCroy 1881M, integration width = 200 nsec). The performance of the crystal prototype was studied with secondary electrons with energy $E_e = 2$ and 4 GeV.

4.5.3 Energy Resolution

The calibration of the calorimeter was performed with 4 GeV electrons by irradiating the centers of each crystal module with a narrow electron beam defined by 2×2 scintillating fiber elements (4×4 mm in size). Then to measure the energy resolution, the centers of both the SIC and BTCP crystal arrays were irradiated with sufficient statistics. We have found a slightly better energy resolution for the SIC crystals. We attribute this to the relatively higher ($\sim 20\%$) light yield of the SIC crystals. For the final energy and position resolution, the central part of the prototype detector was irradiated with 2 and 4 GeV electrons. The reconstructed energy distribution for the 4 GeV electrons is shown in figure 19 for three different calibrated ADC sums: the central module; the inner section comprising 3×3 crystals and the total array of 6×6 crystals. The energy resolution is obtained using a Gaussian fit of the 6×6 distribution. As can be seen in the figure, an excellent energy resolution of $\sigma_E/E = 1.3\%$ has been achieved for 4 GeV electrons. After subtraction of the beam energy spread due to the finite size of the scintillator fibers as well as multiple scattering effects,

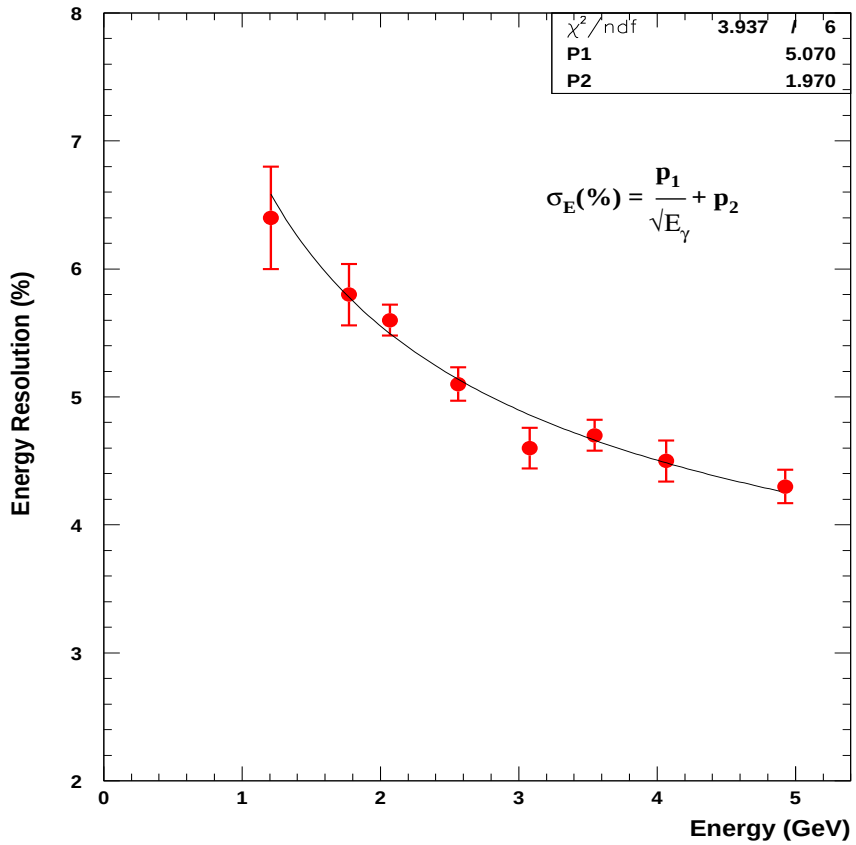

Figure 13: The prototype lead glass detector energy resolution.

this resolution reaches the 1.2% level.

4.5.4 Position Resolution

An important requirement for the HYCAL is the accuracy of the reconstructed position for the decay photons. The impact position of the photons will be determined from the energy of the electromagnetic shower deposited in several neighboring counters. In the case of the $PbWO_4$ crystals, the transverse size of the shower is about two times smaller than that in lead glass. As a result, the position resolution in the $PbWO_4$ detector with an optimal cell size should be two times smaller than lead glass detectors. To maximize the position resolution, we have optimized the crystals' transverse dimension, and have selected it to be $2.05 \times 2.05\ cm^2$. This size is comparable to the Molière radius of the crystal material. The distribution of the reconstructed coordinates for the 4 GeV electrons hitting a crystal cell boundary is shown in figure 20. The linear dependence of the reconstructed coordinates obtained from a logarithmically weighted average of the cell signals, *versus* the impact positions determined by the fiber scintillator detectors is shown in figure 21. As is well known, there is a rather strong correlation between the position resolution (σ_x) and the point at

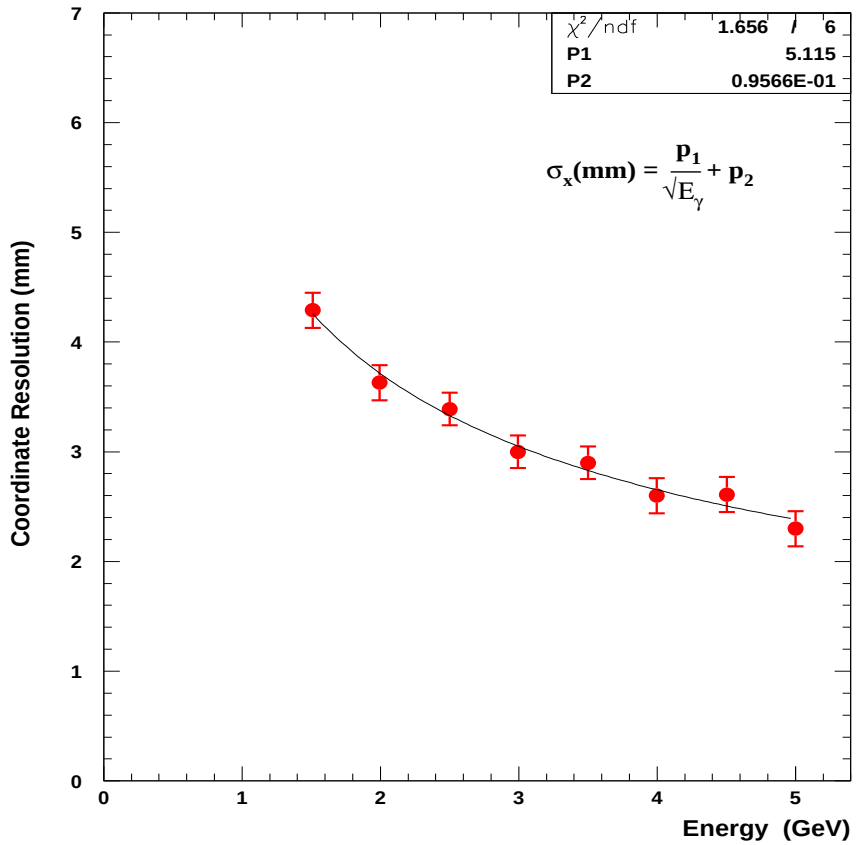

Figure 14: The prototype lead glass detector coordinate resolution.

which the incoming electrons (or photons) hit the detector face. The top plot of the figure shows this dependence for the $PbWO_4$ crystal detectors as obtained from our beam tests. σ_x is smaller (1.28 mm) near the edge of the cell and rises to 2.1 mm in the cell center. These tests showed no measurable difference in the coordinate resolution for the two types of crystals produced by SIC and BTCP.

4.5.5 Gain Change *versus* Radiation Dose Rate

It is well known that all types of crystal scintillators are sensitive to radiation. Because of their fast decay time and high density, $PbWO_4$ crystals were first chosen for use in the CMS and ALICE experiments to construct high precision electromagnetic calorimeters at LHC[24]. The integral radiation level for the CMS experiment is about two orders of magnitude higher than that of the central part of the HYCAL crystal detectors for the PrimEx experiment. For our experiment, the more important characteristic is the change in the crystal response due the radiation dose rate. It was observed experimentally for the earlier crystals that even for a small dose rate ($\sim$ 1 Rad/hour), the gain changes were at the few per cent level. It was understood that this effect is not a result of the change of scintil-

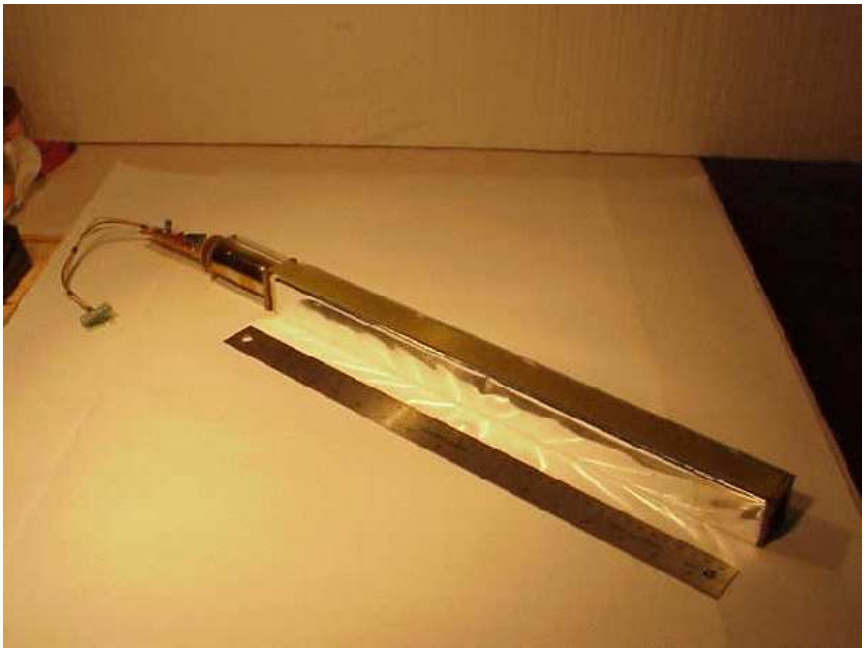

Figure 15: A lead glass detector module.

lation mechanism of the material, but the loss of light output due only to absorption by radiation-induced color centers[25]. This effect has been shown to be clearly correlated with the crystal annealing conditions. A dramatic improvement of this effect has been achieved in recent years by both of the commercial crystal producers. We have done experimental studies of this for each of the two types of crystals produced in the past two years in Russia and China. For these tests, several crystal centers were irradiated with a 4 GeV electron beam at different rates. The duration of each irradiation was kept to about 20 to 30 minutes. The ADC information from all channels of the 6×6 matrix prototype was recorded continuously during the beam irradiation. The normalized pulse height for three typical crystal detectors from each manufacturer is plotted *versus* the relative beam rate in figure 22. The statistical error for each point is shown, and is much bigger for the lower rates for obvious reasons. The plot shows the relative pulse heights as a function of rate for 4 GeV electrons normalized to the 5 kHz point. As is evident from these measurements, we observe opposite behavior for the two types of crystals at high rates. The gain change could be caused by three different effects: (1) the change of the scintillation mechanism in the crystal; (2) the change in the light collection in the radiator; and (3) PMT gain change *versus* rate. Currently, we are in the process of measuring the PMT's performance at similar rates which will allow us to extract this contribution from the experimental data. In any case, our Monte Carlo calcula-

Figure 16: The prototype lead tungstate detector.

tions show that the PrimEx dose rate in the experiment will be equivalent to 10 kHz for 1 GeV electrons or photons. This is twice less than the dose rate for the 5 kHz at 4 GeV point shown on the plot. These rate studies show that both types of crystals can be used for the HYCAL calorimeter in the PrimEx experiment.

4.5.6 The Calorimeter Frame and Transporter

The individual modules of the HYCAL will be assembled in a rectangular box inside of the calorimeter frame. The entire assembly will weigh five tons, and has to be movable in both horizontal and vertical directions in order to place each module in the beam for energy calibration. A transporter has been designed to provide movement of the entire assembly of detectors, its support frame, the thermo-stabilization system, and the delay cables. The light monitoring system will also be mounted on top of the HYCAL frame.

A drawing of the calorimeter in the data taking position is shown in figure 23. In this configuration, the accuracy of centering the detector transverse to the beam will be $\pm 0.7mm$. The calorimeter will be remotely movable so that during calibration, each module can be positioned in the beam of tagged photons with an accuracy of $\pm 2mm$. The system will also

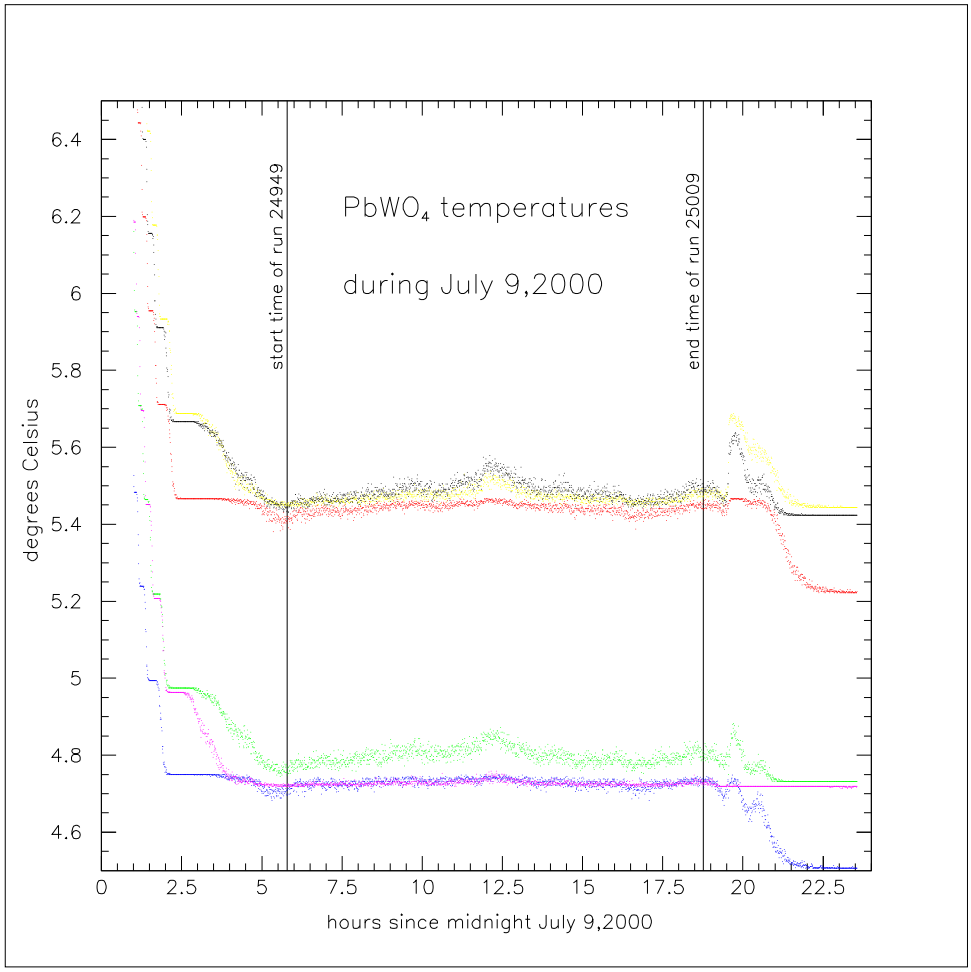

Figure 17: The temperature stability of the lead tungstate crystals during a twelve hour period.

provide the capability to move the detector along the beamline. The conceptual design for this system is shown in figure 24.

When the calorimeter is not being used in the beam, the transporter system will provide positioning of the entire calorimeter a few meters above the beam center on Level 2 of the Hall B Space Frame. In addition to storage, this configuration will allow the HYCAL to be available for assembly, maintenance, and testing with cosmic rays. This design has the advantages of maximizing experimenters' access to the detector while minimizing impact on other Hall B operations.

The conceptual design for the entire system is complete, and the engineering design is currently underway. Some of the components are on order.

4.5.7 The HYCAL Light Monitoring System

The Hybrid Calorimeter has been designed to provide high precision angle and energy information for the detected particles. Angular resolution is required to cleanly distinguish the Primakoff mechanism from π^o production from other processes, and the energy resolution will enable good invariant mass reconstruction for the rejection of background neutral particles. In order to maintain this performance, periodic energy calibration of the HYCAL

Figure 18: A lead tungstate detector module.

with the tagged photon beam will be necessary. This procedure is a time consuming process requiring multiple measurements with the calorimeter in different positions, and therefore cannot be done often. Consequently, an optical monitoring system will be used between successive beam calibrations as a relative calibration.

The main components of the Light Monitoring System (LMS) are a light source, a light mixing box, a light distribution system, reference detectors and a dedicated computer to process the data for continuous stability control. The optical components and the reference detectors are mounted in a thermally insulated aluminum box whose temperature is controlled at a level of 0.1°C. A photograph of the system is shown in figure 25.

The light source comprises an assembly of 31 NICHIA super bright blue LEDs (peak wavelength 470 nm) connected in series. The LED assembly is powered by 150V, 8 nsec pulses generated in an avalanche transistor based circuit. The light pulse width is on the order of 40 nsec which simulates the scintillation response of the lead tungstate crystal. The stability of the light output was observed during a one week period to fluctuate within ±2%. The pulse variations over the period of one measurement (2-5 min) are on the order of (0.2-0.5)%. Pulse to pulse variations are negligible. The prototype light source has

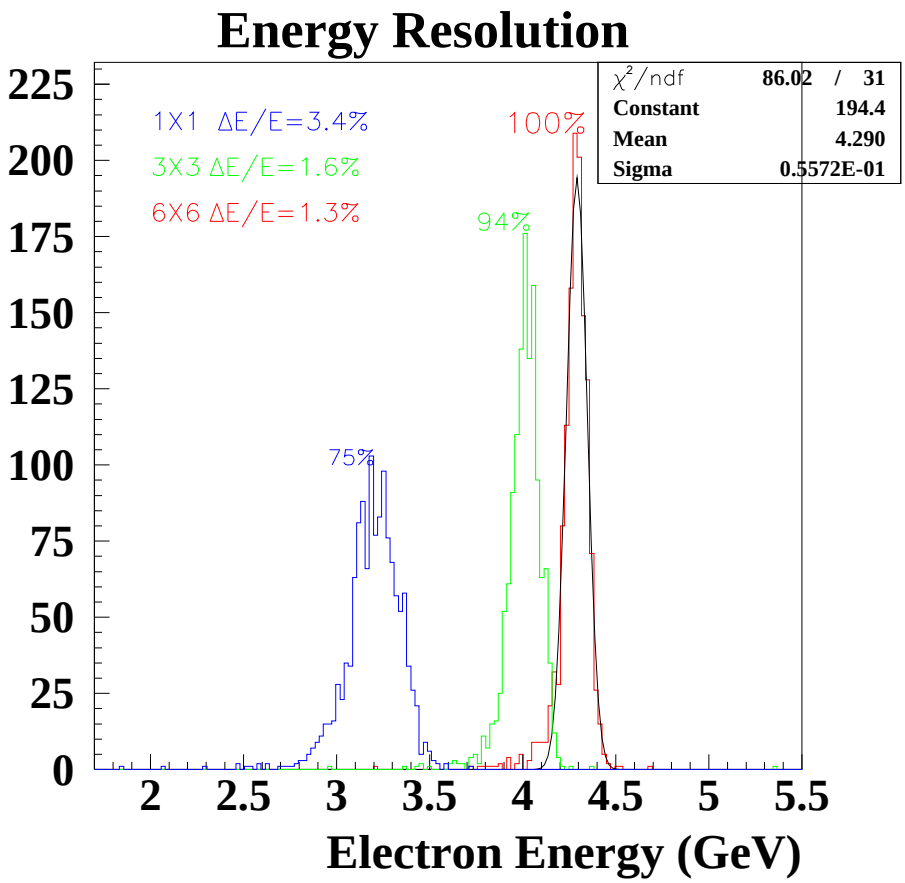

Figure 19: Energy response of a $PbWO_4$ crystal array to 4 GeV electrons. Left peak: single crystal; center peak: 3×3 array; right peak: 6×6 array.

been continuously powered during five consecutive months and no noticeable degradation of performance has been observed. In parallel with the development of the LED based light source, a conventional laser source (nitrogen laser, wavelength 337 nm), along with an assembly of filter wheel and focusing optics and a $10m$ long quartz fiber cable to transmit the light pulse from the laser source to the mixing box, has been purchased and tested. The advantage of the LED based source over the laser based system is in its high reliability and stability. Important advantages are also low maintenance, cost, and low noise level.

Light mixing is necessary for the high precision (sub percent level) monitoring system, as it eliminates the angular and spatial variations of the input light and provides a uniform light output for distribution to the calorimeter channels. For this purpose, a four inch diameter integrating sphere (ORIEL) is being used. For the final design a six inch sphere will be added in order to provide 2000 distribution channels. Light is distributed to the individual calorimeter modules via a bundle of plastic fibers. In order to provide an adequate light pulse for each channel equivalent to the signal of 5 GeV electrons in the calorimeter, we had to attenuate the light after the mixing chamber by a factor of about twenty. The radiation

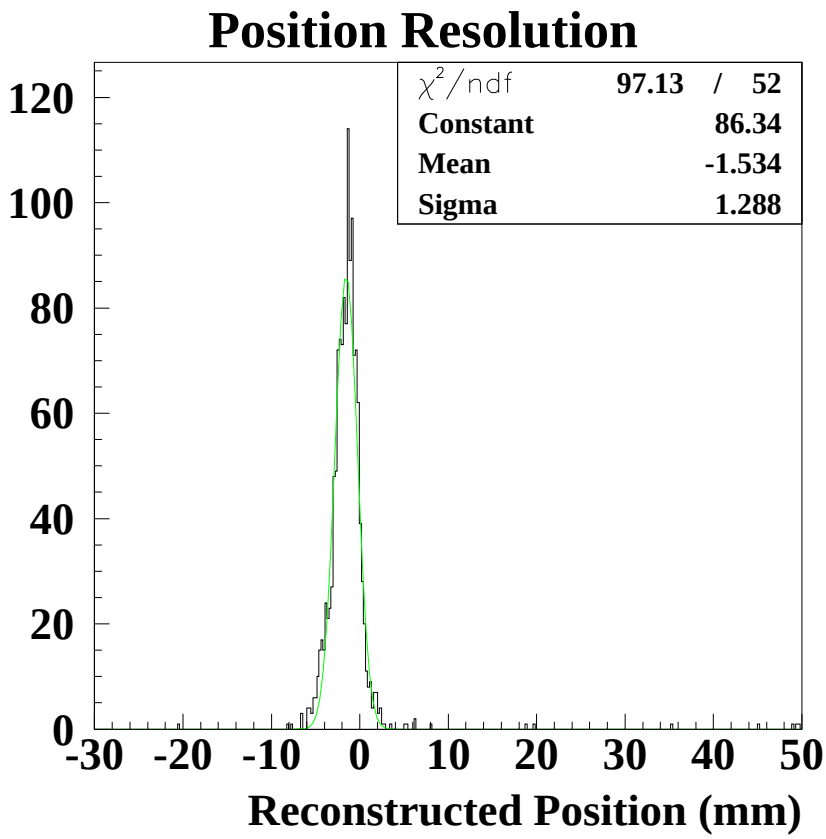

Figure 20: Distribution of reconstructed positions at the boundary between two lead tungstate crystal detectors.

degradation of light transmission in the plastic fiber will be tested during the upcoming June 2002 beam test of the HYCAL prototype. Each fiber from the bundle is terminated on the detector end by a plastic ferrule $10mm$ high and $8mm$ in diameter, with a central hole for the fiber. The fiber tip is permanently glued inside the hole. The ferrule is then attached to the front face of the individual detector module. For stability of light transmission and simplicity of attachment, the ferrules will be glued to the surface using soft UV glue (DYMAX OP-4-20655, bulk modulus 200). This provides a moisture free interface and enables the fiber to be easily disconnected and reattached without damaging the fragile surface of the $PbWO_4$ crystal.

For use as a stable reference detector, three types of photomultiplier tube and a HAMAMATSU PIN photo diode (S3399, 3 mm diameter) with AMPTEC low noise charge amplifier are currently being tested. The reference PIN with the amplifier is mounted directly on the light mixer. The light pulse to the reference photomultiplier tube is transmitted via the fiber cable from the bundle. Each reference PMT is provided with a radioactive alpha-source (Am^{241}) on a scintillating YAP crystal.

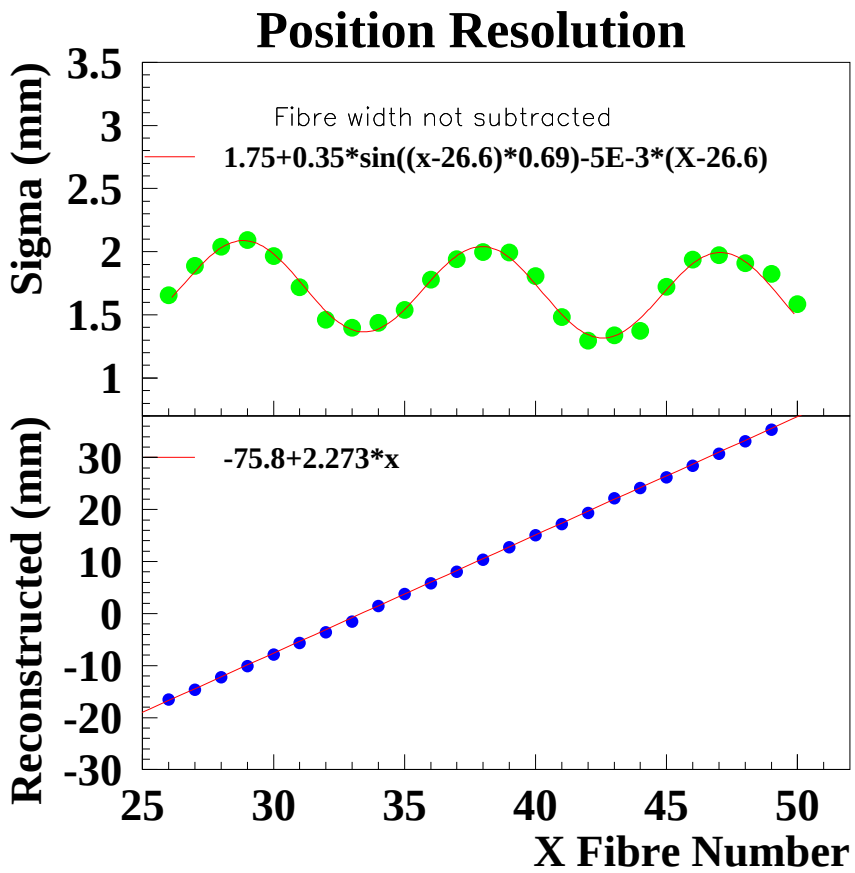

Figure 21: Position resolution (top) and reconstructed *versus* actual position (bottom) across the face of a $PbWO_4$ crystal array.

For the stability measurements the trigger is PMT + "Signal from the pulser" + "Signal from random generator". The PMT signals originate from the YAP scintillation ($\sim$ 80Hz) or light pulses from the light source (10 - 20 Hz). The output from the last dynode of the PMT is used for the trigger. The "Signal from the pulser" is synchronized with the light source pulse generator. The "Signal from random generator" is a random signal of 1 Hz to measure the pedestals.

A CAMAC based Data Acquisition System is being used. LabView DAQ software is used for the readout and on-line analysis. The signals from the reference detectors are digitized in a LeCroy 2249W (11-bit) ADC and read-out through the GPIB-CAMAC interface. The "LMS events" in the calorimeter modules will be read-out in the same way as "real events", *i.e.* electromagnetic showers from real particles. Each type of event will have an ID tag in the data stream. The monitoring system will provide a reference point through an EPICS variable every 2-3 minutes which will be included in the data stream with its proper ID tag. The ratio of the response between the calorimeter photomultipliers and the reference detectors (PMT

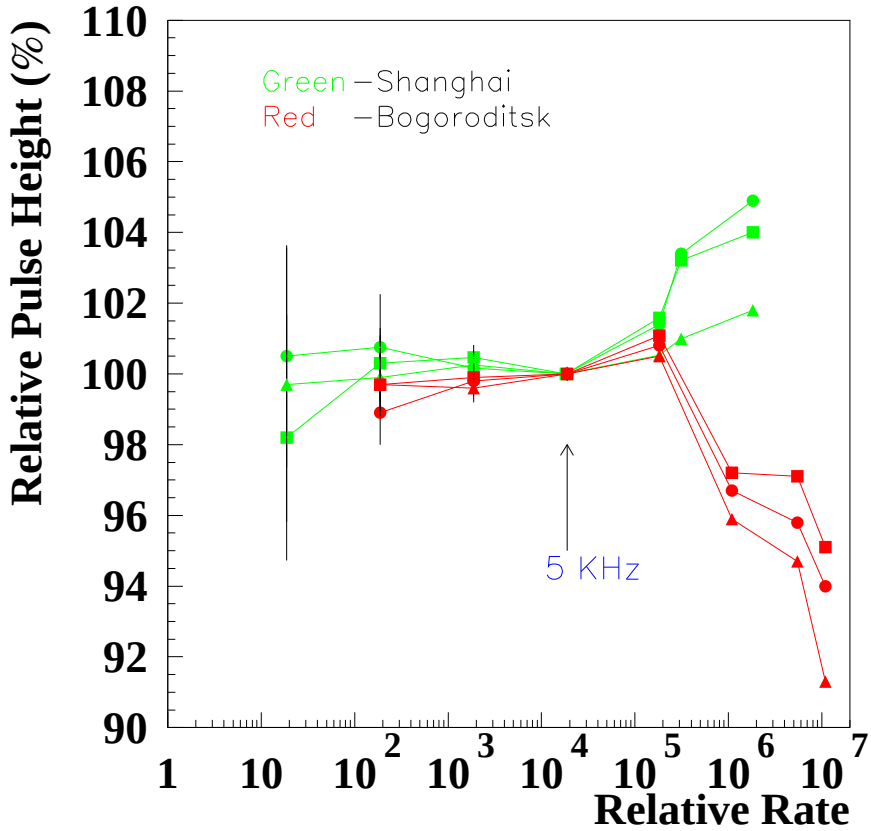

Figure 22: Relative pulse height *versus* rate for Chinese and Russian $PbWO_4$ crystals.

or PIN photo diode) to the "LMS event" will be used to correct the calorimeter response for the "real event".

Light from the light monitoring system will be periodically injected into the detector modules between real events during the data taking. The frequency of the light injection is defined by the optimal performance of the light source and the stability requirement for the $PbWO_4$ crystals. On the basis of experimental tests, the frequency of the light injection has been chosen to be between 10 and 20 Hz. A statistics of 1000-1500 injections ("LMS events") will provide a 0.1% statistical accuracy, which is sufficient to determine a calibration point for each crystal. This will require 100 sec of continuous light injection at 10 Hz. Thus, every couple of minutes we will be able to provide a full relative calibration of the calorimeter.

In a series of prototype stability tests, four signals from three photomultiplier tubes and one PIN diode were digitized, read-out and analyzed. The following quantities have been recorded in the data file: (1) the mean values, standard deviations and the mean value statistical error of each distribution from the LMS light pulse; (2) the same quantities from the three YAP crystals (with the Am^{241} source) for the PMTs; (3) the mean and the width of the pedestals for each channel; (4) the run conditions, such as high voltages, number of

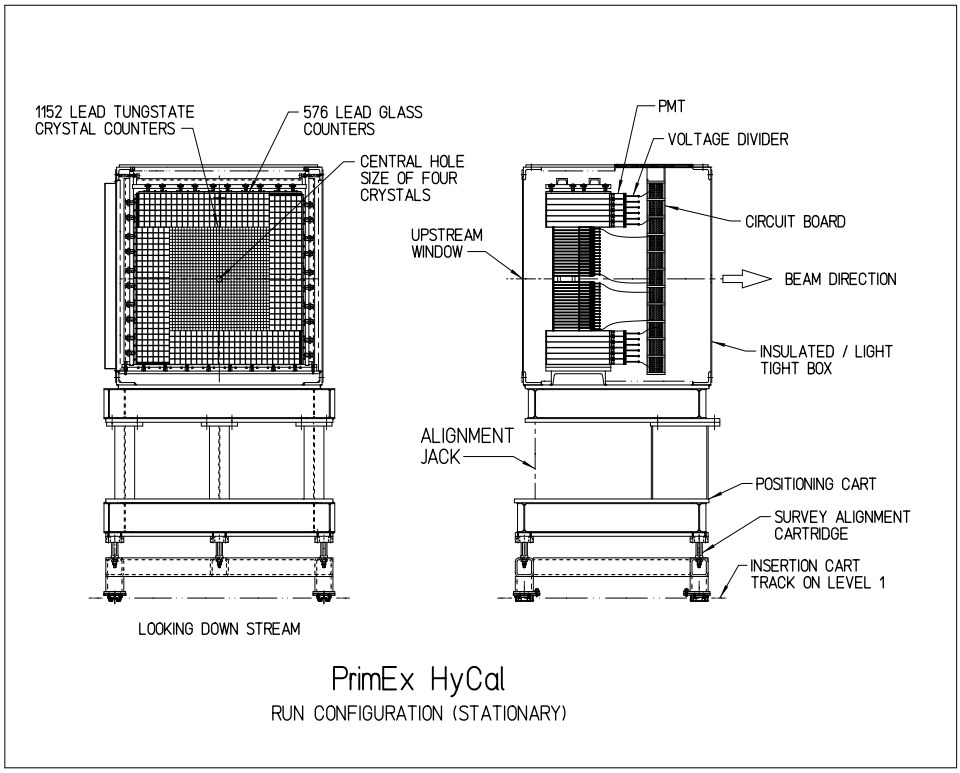

Figure 23: The HYCAL detector on its support stand in the run configuration.

events, the date and time. The mean value of the pulse distribution from the light pulse generator was detected, but not recorded in the file. For the stability factor the following two ratios were calculated: $PIN * YAP_i/LMS_i$ and $(LMS_i/YAP_j)/(LMS_i/YAP_j)$ for the $i-th$ and $j-th$ PMTs, where $i, j = 1, 2, 3$, PIN, LMS and YAP stand for PIN pulse, PMT-light pulse and YAP pulse average. The distribution of the stability over three days is shown in figure 26. The standard deviation of a Gaussian fit to the stability distribution over a three day period is 0.159% (see figure 27).

We plan to test the following aspects of the light monitoring system with beam:

- Radiation hardness of the fibers, LED, and glue.
- Matching of the light signals from the LMS and real particle shower in the $PbWO_4$ crystals. This test will demonstrate how well the injected light reproduces the shower.
- The ability of the LMS to correct for variations in the pulse heights from actual particles resulting from high voltage or beam condition variations.

The prototype system provides up to 700 channels with stable light pulses and is ready for beam tests. The final system will be ready in the fall of 2002.

4.5.8 Veto Scintillators

The veto counters are an array of scintillator paddles in front of the calorimeter that serve to veto charged particle backgrounds. Ten scintillators with PMT readout on both ends will

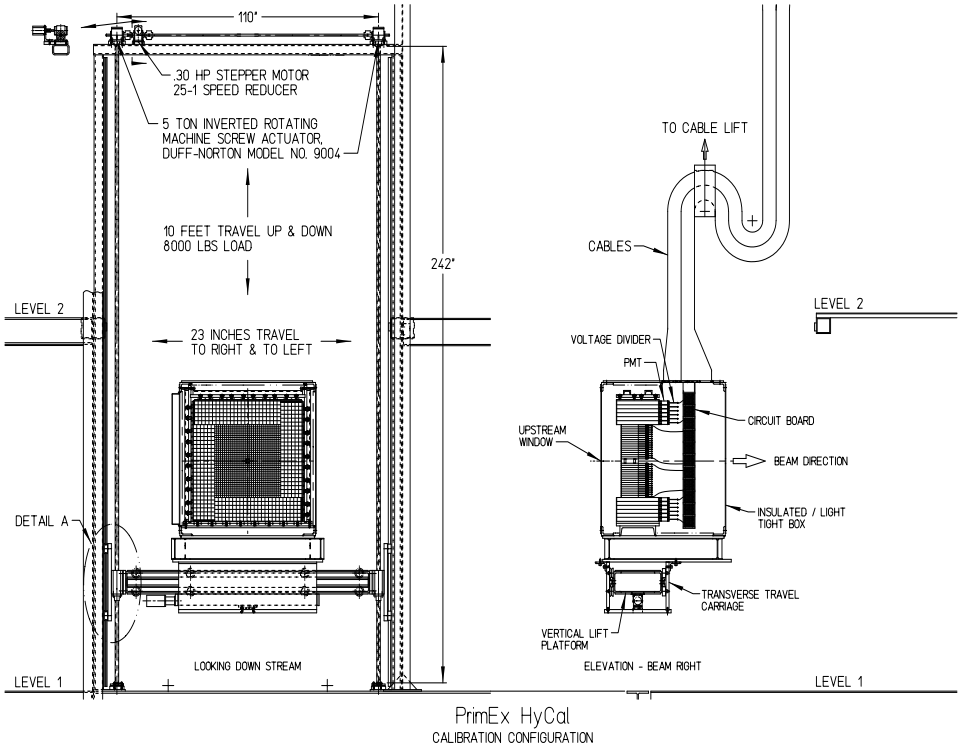

Figure 24: The HYCAL mounted on its transporter.

cover the full solid angle spanned by the calorimeter. In order to minimize photon conversion, only a single 1/4" thick layer of scintillator will be used. Time differences between signals from the two ends of the scintillator will be used to determine the position of the incident particles.

Originally we had planned to construct the veto paddles. However Donal Day from University of Virginia recently volunteered the use of 12 paddles from the UVa G_n^E experiment. The UVa group uses these paddles as charged particle veto counters in front of their large volume neutron detectors, an application similar to ours. The UVa paddles are 1/4" $\times$ 160cm $\times$ 11cm. They have two 2" Phillips 2262B PMT's mounted on them using the CERN housing. The expectation is that the UVa counters will be adequate for our purpose. Since the G_n^E experiment pushed these detectors extremely hard in terms of count rate, we have reserved MRI funds so that the PMT's can be replaced if necessary. We are also considering shortening the scintillators since they are approximately 50cm longer than necessary. A beam test scheduled for June 2002 should help clarify what modifications, if any, are needed to the veto counters. Recently one of the counters was shipped to the University of Massachusetts and bench testing of the detector using cosmic rays has started.

4.6 Electronics and Data Acquisition

The PrimEx DAQ system must read out over 2200 channels of ADC and TDC information coming from five different detector systems. These include the HYCAL calorimeter, the HYCAL veto, the pair spectrometer, the total absorption counter, and the Hall-B photon

Figure 25: The prototype light monitoring system.

tagger. The digitization electronics will span at least three Fastbus crates which must be coordinated for proper event reconstruction.

The PrimEx DAQ system is a CODA based Fastbus system utilizing the JLab designed Trigger Supervisor module. In addition to the three Fastbus crates, this system includes one CAMAC crate, one VME crate, and one hybrid VME/VXI crate. Electronics occupying six NIM crates are also needed for the first stages of the trigger. A diagram of the DAQ system can be seen in figure 28. A big advantage of the CODA/Trigger Supervisor system is the ability to run in fully buffered mode. In this mode, events are buffered in the digitization modules themselves allowing the modules to be "live" while being readout. This significantly decreases the deadtime of the experiment. It is particularly important to have a low deadtime for PrimEx given that the expected π^o production rate is only 0.11 Hz.

A major portion of the electronics needed for the PrimEx DAQ and trigger electronics has been procured and is onsite at JLab. A list of the major components can be seen in table 1.

4.6.1 High Voltage

An order for 1228 channels of high voltage was placed with CAEN in December 2000 at a total cost of $134.5k. The HV will be used to power the photomultiplier tubes for HYCAL

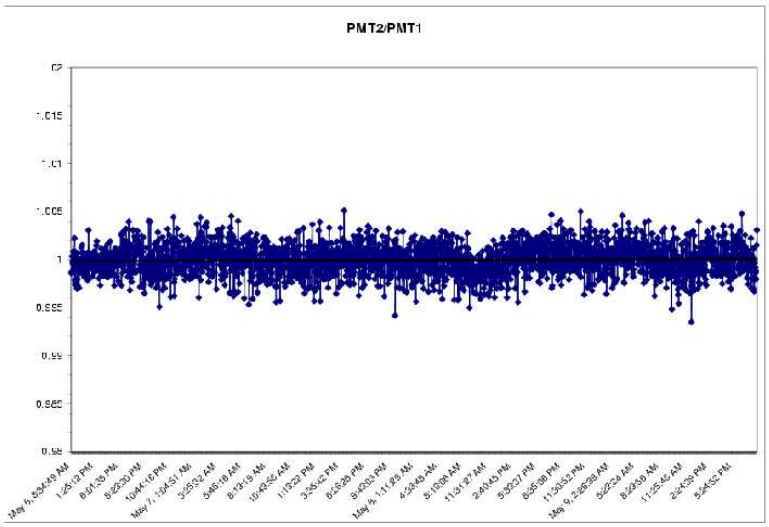

Figure 26: Stability of the prototype light monitoring system over three days.

and the veto counters. The four mainframes that house the HV modules were delivered in the summer of 2001 and have been tested and checked out. In late 2001, we received prototype 28 and 48-channel HV modules from CAEN which have been tested. The overall performance of the modules was as anticipated, although some technical glitches/questions were reported to CAEN. Since then we have received the one production 28-channel module that was ordered, and are waiting for delivery to start on the 25 48-channel modules that were ordered. CAEN anticipates they will start delivering the 48-channel modules in early June of 2002.

Since late 2000 when the HV order to CAEN was placed, the number of detector channels in HYCAL has increased by approximately 400 with the expansion of the size of the central high resolution region. Provided that the CAEN HV system performs as anticipated, we expect to order an additional 12 units of the 48-channel HV module and another HV mainframe from CAEN. MRI funds for this are being held in reserve.

The CAEN HV system uses a multi-conductor HV cable with multi-pin HV connector. The HV connectors were developed at CERN for use on the LHC, and are produced commercially by a French firm called Radiall-Jerrik. We and most other end users have had serious problems in using these connectors to make HV cables. The problem has been reported to Radiall-Jerrik and they are working on a technical fix. Meanwhile, all the connector parts

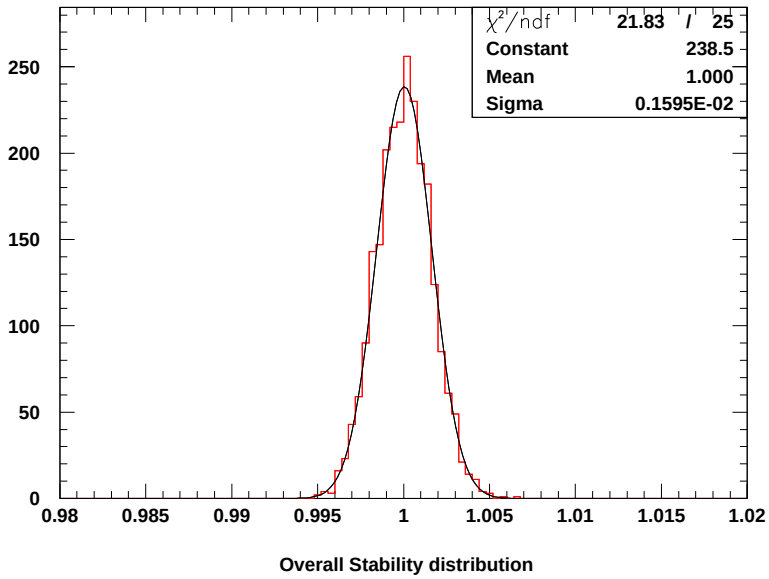

Figure 27: The stability distribution of the light monitoring system over three days.

that we purchased have been returned and at the present time we are waiting for the delivery of new parts. Our understanding is that Radiall-Jerrik expects to ship replacement parts in late May of 2002.

4.6.2 Trigger and HV Slow-Controls

We have started the development of a PC based LabView system for control of the HV and the trigger electronics. The status of the HV system has been described previously. Here, the status of that portion of the trigger electronics that is computer-configurable is described.

The user controlled parts of the trigger are the trigger logic unit and DAC, both of which are housed in a CAMAC crate in Hall B. The trigger logic unit is used to set the trigger condition for HYCAL, *i.e.* which combinations of energy sums must be over threshold in order to trigger the experiment. The DAC is used to set thresholds for the energy sums. We control these instruments remotely over the internet through a Kinetic Systems GPIB CAMAC controller and a National Instruments GPIB E-Net device. Recently this system was shipped to JLab for installation in Hall B.

We also evaluated the LeCroy 2373 16-bit MLU and the CAEN C542 8-bit programmable logic unit for possible use in PrimEx. Hall A and other groups have recently reported that the LRS 2373 can exhibit large non-linear dead-time effects. However, bench testing did not

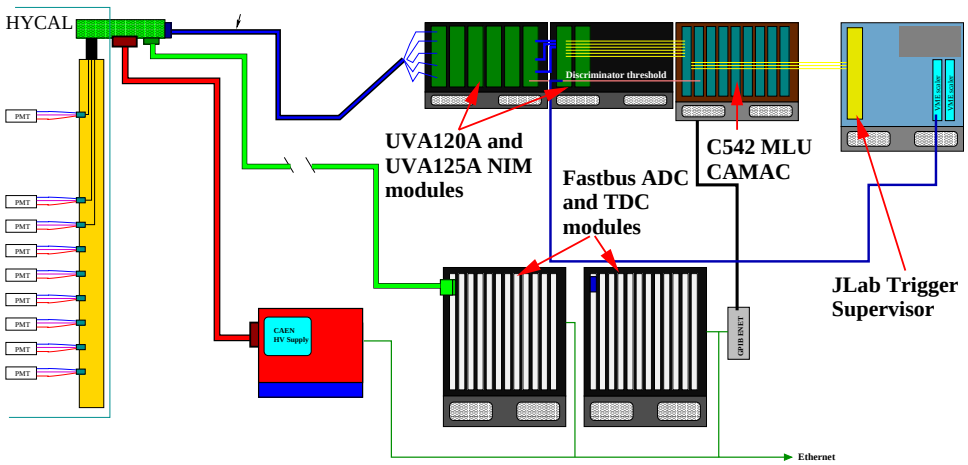

Figure 28: Diagram of the PrimEx DAQ system. The trigger is formed using only the last stage dynode signals from HYCAL (left side). The anode signals are sent directly to the Fastbus ADC modules via long RG58 coaxial delay lines. The system is controlled by a JLab designed Trigger Supervisor module (far right).

Item	**# in hand**	**Total # Needed**
LRS 1881M ADC, Fastbus	24	28
LRS 1877 TDC, Fastbus	1	1
UVA120A Linear fan-in, NIM	13	52
UVA125A Fan-in/discr., NIM	5	6
Fastbus crate w/ power supply	2	2
CAMAC crate	1	1
Trigger Supervisor-2, VXI	1	1
VXI/VME hybrid crate	1	1

Table 1: Partial list of major electronics items required for PrimEx.

show evidence for any anomalous behavior, provided that additional strobes do not occur within the 59 ns conversion time of the module. The CAEN unit has a conversion time of 14 ns in strobed mode. Because of the shorter conversion time of the CAEN module, and subsequent need for less ADC delay cable, we will use the CAEN logic unit in PrimEx.

4.6.3 Custom Delay and Trigger Cables

The original design of the PrimEx DAQ system left open the possibility of using analog delay chips rather than traditional coaxial delay cable. A study of the DDD2211 analog delay chip *versus* an RG58 coax cable was performed. The results of this study coupled with financial considerations and the availability of existing cable led us to the decision to use RG58 coax for signal delay.

With the upgraded number of channels in HYCAL (1728), a total of about 3500 RG58 cables are needed to carry both the dynode and anode signals to the trigger and digitization electronics. Considering the requirement that HYCAL be compact enough to allow for over

a meter of motion in two directions, there is scarcely enough surface area on the HYCAL enclosure for this many coaxial connectors. A solution incorporating mass termination of a number of channels (32-36) is being implemented instead. Custom printed circuit boards (PCBs) have been designed and will be tested with the HYCAL prototype in the summer of 2002. These boards have short traces that connect the solder pad for the RG58 cable to a board mounted connector. This not only makes for a more compact design, but will significantly decrease the load-in time.

4.6.4 Trigger Design

The PrimEx trigger will look for multiple clusters in HYCAL separated by at least $15cm$. This will be done by fanning in strips of like detectors ($PbWO_4$ and Pb-glass will be done separately) which span the calorimeter. Using strips in this fashion ensures at least 50% of the energy deposited in one cluster will be seen by a discriminator. Alternate geometries would lead to smaller percentages and would require splitting the dynode signals into more than two channels.

The UVA120 linear fan-in module was chosen for the PrimEx trigger because of its large number of channels (36) and the economic advantage over commercial modules. The specific needs of the PrimEx trigger required some special modifications to both the UVA120 and its sister module, the UVA125. One significant modification in the UVA120A design was to make both outputs inverting. This allows the module itself to be used as both a splitter and an inverter for the dynode signals, eliminating the need for additional hardware.

The core of the trigger logic will be performed by the CAEN C542 CAMAC MLU. This module was tested along with the LRS2373 unit and found to be the best choice for the PrimEx trigger. The trigger design will incorporate three of the C542 units, eliminating the need for several NIM modules while simplifying the wiring. This also gives greater flexibility in modifying the trigger from the counting house.

4.6.5 Expected Background and Trigger Rates

With the modifications required for the trigger due to the new geometry of HYCAL, a new Monte Carlo study was performed to estimate the acceptance efficiencies and trigger rates. The new study has several improvements over the original one including energy smearing, a more accurate beamline definition, more realistic detector geometry, and realistic bremsstrahlung angular distribution.

The first part of the study focused on the trigger's acceptance efficiency for Primakoff π^o events. The programming of the C542 MLU units was emulated in software so that the algorithm could be fully tested. Figure 29 shows the event viewer used to analyze simulated data. The acceptance efficiency is expected to be nearly 100% for π^o decays whose photons each have a given minimum energy (determined by discriminator threshold settings) and have trajectories pointing to the fiducial part of HYCAL. The few trigger failures expected are due to energy leakage through the cracks between detectors in HYCAL. Figure 30 shows a plot of the trigger efficiency *versus* the minimum decay photon energy if the trigger were set to accept all 500 MeV or greater photons. This plot shows that the triggering efficiency is quite insensitive to the discriminator threshold.

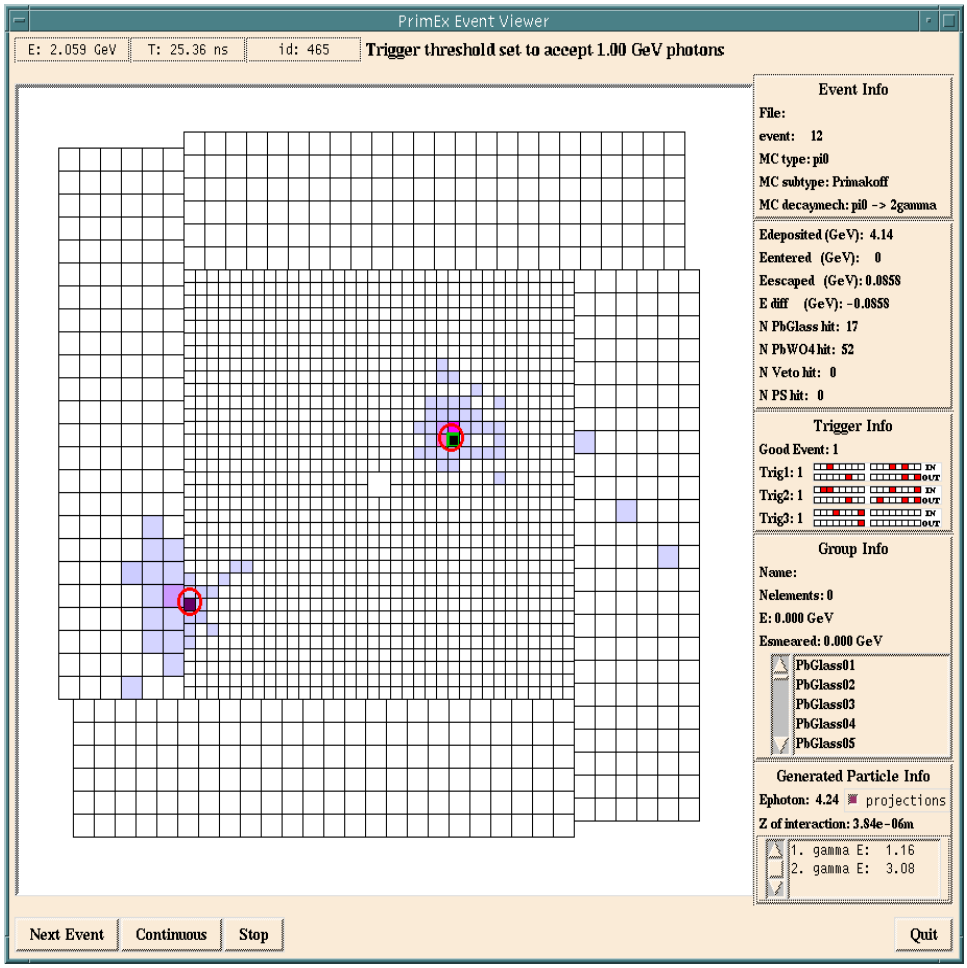

Figure 29: PrimEx event viewer for Monte Carlo data. This is used to diagnose individual events and the trigger's response.

The second part of the Monte Carlo study focused on estimating the trigger and detector rates due to backgrounds and accidentals. Figure 31 shows an upper limit on the PrimEx trigger rate as a function of the decay photon energy, estimated by simulation. This upper limit was calculated assuming a 50 ns coincidence window. In reality, PrimEx will use something closer to 20 ns. A "worst case scenario", however, was employed in order to obtain a believable upper limit. An arrow on the plot indicates the 750 MeV photon energy point with an event rate of approximately 1.5 kHz. Unlike the triggering efficiency, the background rate is very sensitive to the value of the discriminator thresholds. For the actual experiment, the thresholds will be set as low as possible such that the deadtime does not exceed 5%.

The primary contribution to background rates come from two sources: (1) e^+e^- pair production upstream of the helium bag and (2) Compton scattering from the helium itself. Figure 32 shows the sources of these backgrounds along the beamline. Backgrounds originating in the beam pipe are due to large angle bremsstrahlung photons showering in the beam

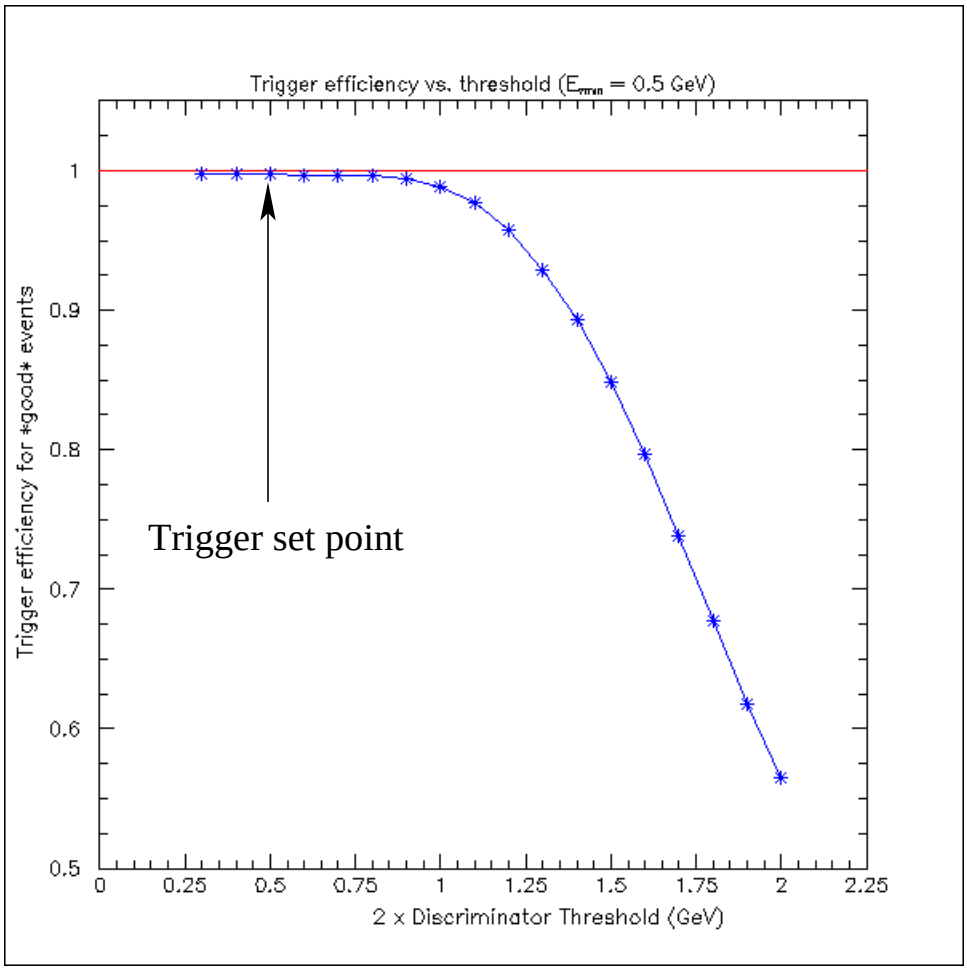

Figure 30: Plot of the trigger acceptance efficiency (estimated from simulation) *versus* discriminator threshold. The acceptance efficiency is based on accepting 500 MeV or greater photons. The arrow indicates where the threshold should be set for accepting 500 MeV photons. The curve shows that the acceptance efficiency is very insensitive to the discriminator threshold.

pipe. Occasionally, some energetic shower photons will pass down the beamline, through the magnet, and into HYCAL. This type of event will be easily rejected in software.

Further simulation studies estimated discriminator rates and detector rates. The expected discriminator rates are shown in figure 33 for the $PbWO_4$ detector strips. The rates corresponding to the minimum decay photon energy of 750 MeV (initial PrimEx trigger point) for the innermost strips will fire at less than 10 kHz.

Figure 34 shows the integrated detector rates as a function of energy deposited for $PbWO_4$ crystals at various distances from the beamline. The highest curve corresponds to the detectors which line the beam hole in the center of HYCAL. These are non-fiducial detectors and will see 1 MeV or more energy deposition at a rate of 200 kHz. Energy of 1 GeV or more will be deposited in one of these detectors at a rate of a few kHz. The bump on the high energy end of the top curve comes from e^+e^- pairs produced in the mylar window

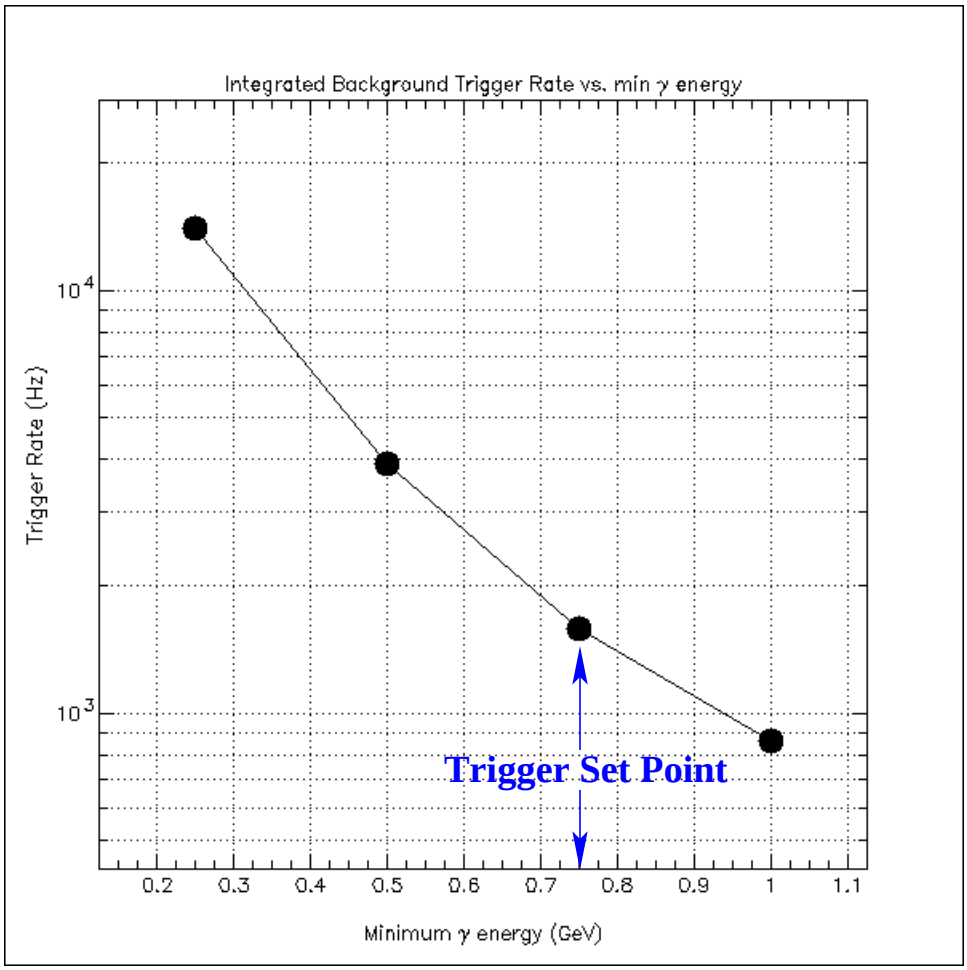

Figure 31: Trigger rate (upper limit) due to background *versus* the minimum decay photon energy. The rate includes accidentals from combining several background events. The discriminator values will initially be set to correspond to the 750 MeV decay photon energy point. The final discriminator values will be determined by the deadtime in the DAQ system.

on the upstream end of the helium bag. Only a few of these pairs have a particle produced at a steep enough angle to hit HYCAL.

4.7 Energy Calibration

The collaboration is pursuing a number of methods to determine the absolute energy calibration of the tagged photons. Two of the methods rely on the fact that the energy of the electron beam will be determined to an accuracy of 2×10^{-4} using the Hall A arc section. To calibrate the tagger, we plan to employ a technique utilizing the pair production luminosity monitor. The magnetic field of the sweep dipole will be adjusted to the maximum value at which there is some acceptance for e^+e^- coincidences. The sweep dipole field will then be lowered, and the field at which e^+e^- pairs just begin to come in coincidence with a given tagging counter (corresponding to symmetric energy sharing in pair production) will be noted. Under the assumption that the $\int B \cdot dl$ of the pair spectrometer dipole varies linearly with

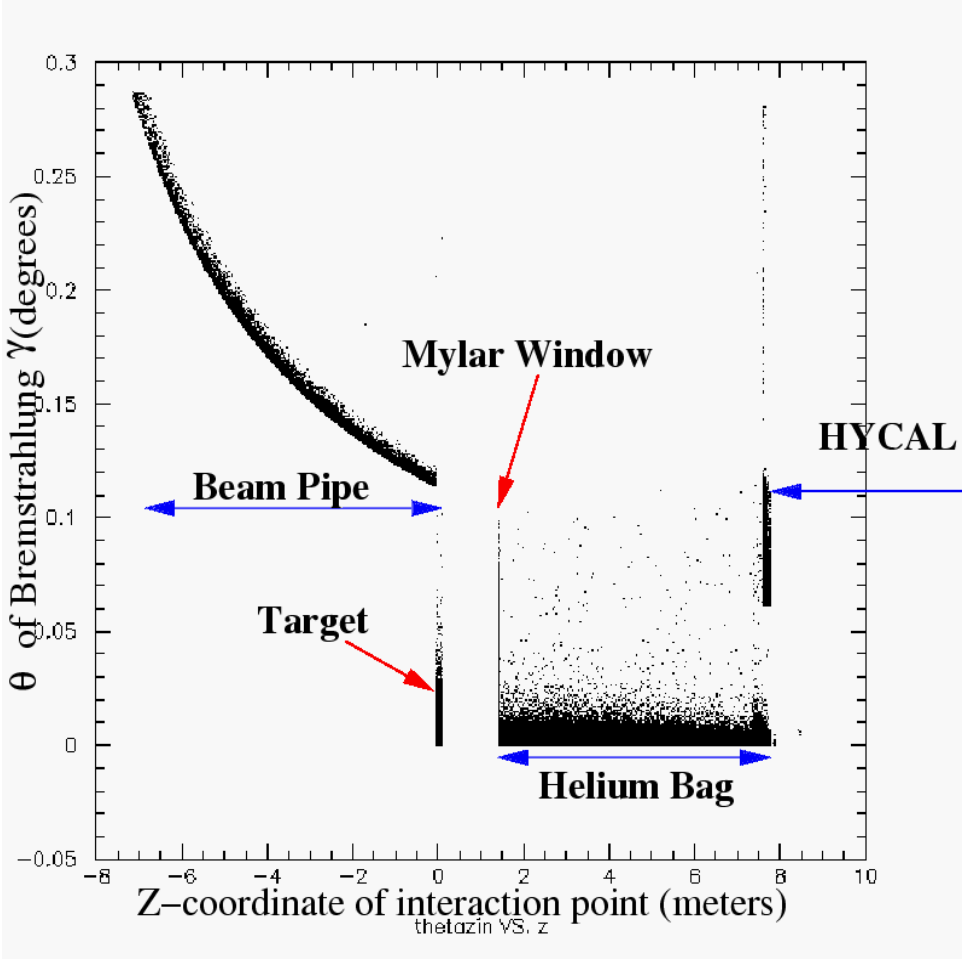

Figure 32: Location of background sources along Hall B beamline. The angle of the bremsstrahlung generated beam photon is plotted *versus* the position along the beamline at which the initial interaction took place. The relevant beamline components included in the simulation are shown.

the central field of the dipole as measured by an NMR probe, one can determine the energy of a given tagging counter with respect to the endpoint energy. To this end, the field of the pair spectrometer dipole has been carefully mapped. The implementation of this technique will require position sensitive detectors with high spatial resolution ($\sim 400\mu m$) to measure the e^+e^- pairs. With the addition of a new low current beam dump in the Hall one could also measure the tagged photon energy with respect to the electron beam, as opposed to its bremsstrahlung endpoint, with an analogous method. These options are under study.

The ability to detect e^+e^- pairs with high resolution has advantages beyond absolute energy calibration. Gil and Oset[22] have suggested that $A(e, e'\gamma)X$ processes in the bremsstrahlung converter, incoherent bremsstrahlung, may set limits on the tagging technique at high energies. Similarly, the emission of soft photons in addition to the high energy photon emitted in the bremsstrahlung process[23], double bremsstrahlung, will also weaken the correlation in energy between the bremsstrahlung photon and the post-bremsstrahlung

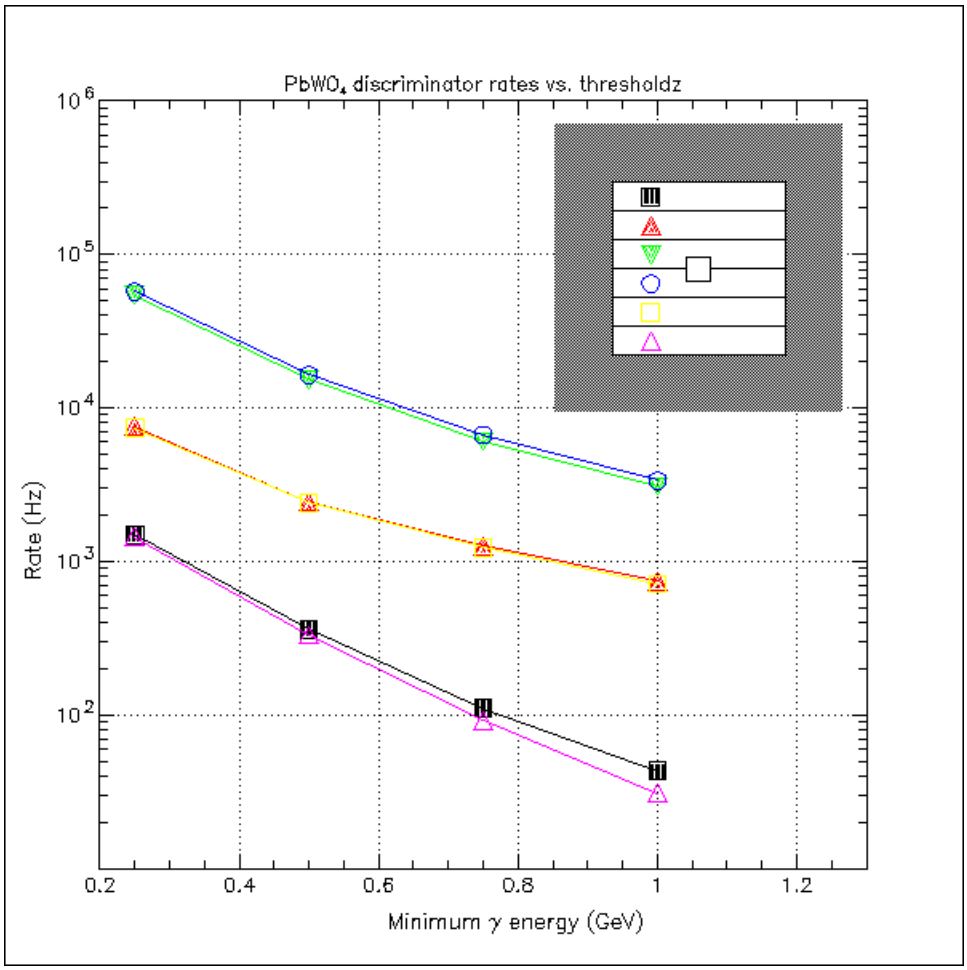

Figure 33: Discriminator rates for $PbWO_4$ detectors in HYCAL as a function of the minimum decay photon energy. The discriminator thresholds will be defined as half of the minimum decay photon energy. The initial setting of the threshold will be set to the point corresponding to 750 MeV on the x-axis. The maximum discriminator rate expected for this setting is less than 10 kHz.

electron in the tagger. A high resolution e^+e^- detection system will enable the study of such effects.

We are also studying a technique in which the energy of the tagged photon beam is calibrated at the 10^{-3} level via electron Compton scattering near the minimum opening angle. The opening angle ($\psi_{\gamma e} = \theta_\gamma + \theta_e$) between the recoil electron and the scattered photon reaches a minimum in the kinematic region where the partial derivative $\frac{\partial E_\gamma(\psi_{\gamma e}, \theta_\gamma)}{\partial \theta_\gamma} = 0$. In this case, the determination of the incident photon energy is independent of the beam direction, $\Delta\alpha$, to first order:

$$E_\gamma(\psi_{\gamma e}, \theta_\gamma + \Delta\alpha) = E_\gamma(\psi_{\gamma e}, \theta_\gamma) + \Delta\alpha \frac{\partial E_\gamma(\psi_{\gamma e}, \theta_\gamma)}{\partial \theta_\gamma} + \Theta(\Delta\alpha^2) \tag{10}$$

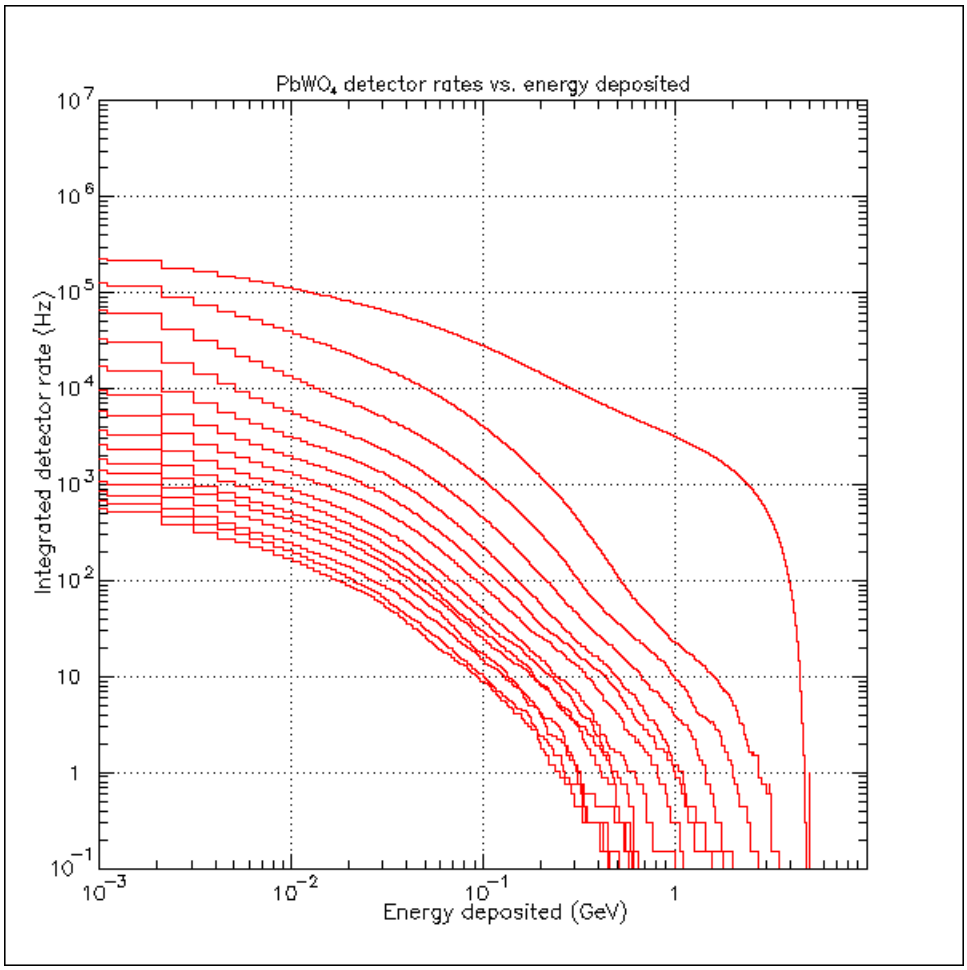

Figure 34: Integrated detector rates *versus* lower energy limit. The rates (Y-axis) are determined by integrating the rates from a lower limit (X-axis) to the beam energy. The different curves correspond to detectors at various distances from the beamline. The highest rates are detectors closest to the beamline while the lowest rates are detectors furthest from the beamline.

When $\frac{\partial E_\gamma(\psi_{\gamma e},\theta_\gamma)}{\partial \theta_\gamma} = 0$, the relation becomes:

$$E_\gamma(\psi_{\gamma e}, \theta_\gamma + \Delta\alpha) = E_\gamma(\psi_{\gamma e}, \theta_\gamma) + \Theta(\Delta\alpha^2) \tag{11}$$

If one selects the Compton events in the region near the minimum opening angle, the energy measurement is not sensitive to the systematic uncertainty of the beam direction. We will therefore determine the absolute photon beam energy by measuring the electron and photon scattering angles near the minimum opening angle.

We simulated the beam energy measurement for a 2×10^7 equivalent γ/sec beam intensity on a 10^{-3} radiation length ^9Be target for a five day running period. The overlap of two E counters in the photon tagger will provide a $\sim 10^{-3}$ energy bin. The following conditions are included in the calculation:

- initial photon beam energies, E_γ are 4.995, 5.000, 5.005 and 5.010 GeV;
- HYCAL is 12 meters downstream of the target;
- lead tungstate crystal calorimeter resolution;
- multiple scattering on a 0.1% radiation length ^9Be target;
- electron atomic motion effect in ^9Be;
- beam spot size: $\sigma_x = \sigma_y = 0.7$ mm;
- detector misalignment $\Delta x = \Delta y = 1$ mm;
- assumed misalignment of the beam: $\theta = 10^{-4}$ rad, $\phi = 0.785$ rad.

Figure 35 shows the Monte Carlo simulations for four different initial beam energies (4.995, 5.000, 5.005 and 5.010 GeV) under the conditions listed above. As can be seen, for each step of 0.005 GeV in the initial beam energy shift, the reconstructed beam energy gives the correct answer within an error of $\frac{\Delta E}{E} \sim 10^{-3}$.

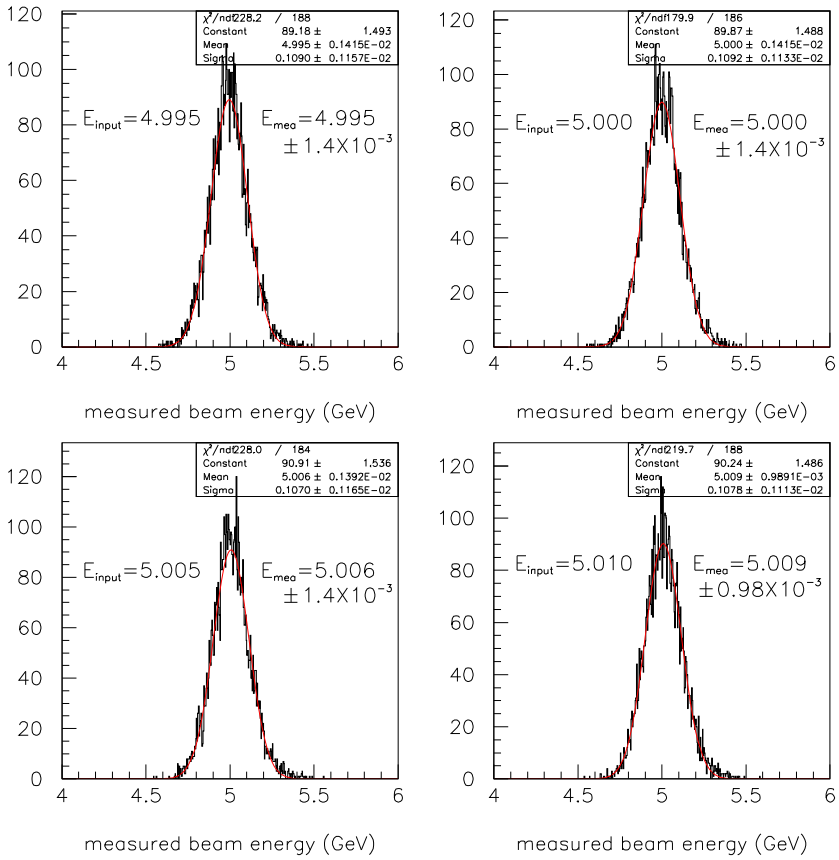

Figure 35: Monte Carlo simulation of the measured beam energy distribution for four different initial beam energies, 4.995, 5.000, 5.005 and 5.010 GeV. A kinematic cut, $\psi_{\gamma e} < 2.1^o$, is applied to all plots.

5 Summary

We are requesting the continued support of the Jefferson Laboratory management for our efforts to perform a precision test of the axial anomaly in quantum chromodynamics. The fundamental importance of this experiment is evidenced by the fact that in anticipation of the results, three independent theoretical calculations of the chiral corrections to the decay rate have been performed. These next-to-leading order corrections have indicated an increase in the width by approximately 4%. In our view, this provides an increased impetus to perform a measurement of this width with a precision commensurate with the theoretical knowledge. The PrimEx Collaboration is at present the only collaboration in a position to perform these measurements.

The Collaboration has made significant strides towards getting this experiment ready to run. Some of the major accomplishments at this point are:

- Secured $\sim \$1,000,000$ funding through a Major Research Instrumentation grant from the National Science Foundation (PHY-0079840) for development of the PrimEx experimental setup. Approximately 75% of these funds have been spent for procurement of equipment.
- A new Total Absorption Counter (TAC) has been designed and constructed for a high precision determination of the tagger efficiency. The first stage of commissioning with beam has been performed.
- A new harp has been designed, constructed, and commissioned for precise photon beam monitoring.
- Developed a procedure to measure the Primakoff target thicknesses at the 0.7% level and have designed and constructed the PrimEx target ladder.
- Designed, constructed and installed the PrimEx/Hall B Pair Spectrometer for photon flux monitoring at the 1% level. Commissioning of this device is currently underway.
- Completed research and development work for the HYCAL calorimeter. Beam tests for several prototype lead glass detectors and $PbWO_4$ crystals are completed. High energy and position resolutions have been achieved. Manufacturer for crystals has been selected and procurement of 1200 $PbWO_4$ crystals is complete. Currently 800 crystals are on site, with the remaining crystals scheduled to arrive in July 2002. Lead glass modules have been selected. 1000 modules with PMT's and high voltage dividers are on site.
- Photomultiplier tubes for the $PbWO_4$ crystals detectors have been selected. 1200 have been purchased and are currently on site. High voltage dividers are designed, and their construction is complete.
- Designed and tested a light-based gain monitoring system for the Hybrid Calorimeter.
- Conceptual design of the HYCAL frame with transporter is complete. Engineering design is currently underway. The frame and transporter is scheduled to be ready for HYCAL assembly in the Test Lab in Fall 2002 for cosmic ray tests.

- Procured veto scintillators for the Hybrid Calorimeter.
- Designed the data acquisition electronics and slow controls systems, and have completed procurement of most of the components.
- Refined our studies of trigger efficiencies and backgrounds.
- Two alternate techniques for high precision tagged photon beam energy calibration are currently being developed. A proposal to measure forward electron Compton scattering with the PrimEx setup for the energy calibration has been submitted to PAC22 as a Letter of Intent.

The PrimEx experiment is in full development phase. The experimental setup is planned to be ready for installation in Hall B during the first part of 2003. It is the intention of the Collaboration to run this experiment during the second part of 2003. As such, we are renewing our request for 22 days of 6 GeV beam time in Hall B, as was approved by PAC15.

References

[1] See *e.g.* Dynamics of the Standard Model, J.F. Donoghue, E. Golowich, and B.R. Holstein, Cambridge University Press (1992).

[2] J.S. Bell and R. Jaciw, Nuovo Cimento 60A, 47 (1969). S.L. Adler, Phys. Rev. 177, 2426 (1969).

[3] R.M. Barnett *et al.*, Review of Particle Physics, Phys. Rev. D54,1 (1996).

[4] J. Bijnens, A. Bramon and F. Cornet, Phys. Rev. Lett. 61 (1988) 1453.

[5] J.F. Donoghue, B.R. Holstein, Y.C.R. Lin, Phys. Rev. Lett., vol. 55, (1985), 2766; J.F. Donoghue, B. Wyler, Nucl. Phys., B316, (1989), 289.

[6] H. Leutwyler, Phys. Lett. **B378** (1996) 313 and hep-ph/9602255.

[7] J. L. Goity, A. M. Bernstein, J. F. Donoghue, and B. R. Holstein, manuscript in preparation; J. L. Goity, talk at Baryons 2002.

[8] B. Ananthanarayan and B. Moussallam, preprint hep-ph/0205232.

[9] H. Leutwyler, private communication.

[10] B. Moussallam, Phys. Rev. **D51** (1995) 4939.

[11] G. von Dardel *et al.*, Phys. Lett., vol. 4, no. 1, (1963), 51.

[12] D.A. Williams *et al.*, Phys. Rev. D, vol. 38, no. 5, (1988), 1365.

[13] H.W. Atherton *et al.*, Phys. Lett., vol. 158B, no. 1, (1985), 81.

[14] H. Primakoff, Phys. Rev. 81, 899 (1951).

[15] A.M. Bernstein, Nucl. Phys. A623 (1997) 178c.

[16] G. Bellettini et al., Il Nuovo Cimento, vol. 66, no. 1, (1970), 243.

[17] V.I. Kryshkin *et al.*, Sov. Phys. JETP, vol. 30, no. 6, (1970),1037.

[18] G. Bellettini *et al.*, Il Nuovo Cimento, vol. 40, no. 4, (1965), 1139.

[19] A. Browman *et al.*, Phys. Rev. Lett., vol. 32(1974) 1067.

[20] A. Browman et al., Phys. Rev. Letts., vol. 33, no. 23, (1974), 1400.

[21] Available at the PrimEx web site: http://www.jlab.org/primex/

[22] A. Gil and E. Oset, Nucl. Phys. A580, (1994) 517.

[23] K. Mork and H. Olsen, Phys. Rev., vol 140, number 6B, (1965), B1661.

[24] Compact Muon Solenoid Technical Proposal, CERN/LHCC 94-38, LHCC/P1, (1994).

[25] R.Y. Zhu, et. al. IEEE Transactions on Nuclear Science, v.45, no.3,(1998).